Science of the Total Environment 858 (2023) 160078

Contents lists available at ScienceDirect

Science of the Total Environment

journal homepage: www.elsevier.com/locate/scitotenv

Ferroptosis contributes to nickel-induced developmental neurotoxicity in zebrafish

Zuo Wang [a], Kemin Li [a], Yanyi Xu [a], Zan Song [a], Xianyong Lan [b], Chuanying Pan [b], Shengxiang Zhang [a], Nicholas S. Foulkes [c], Haiyu Zhao [a,*]

[a] School of Life Sciences, Gansu Key Laboratory of Biomonitoring and Bioremediation for Environmental Pollution, Lanzhou University, No. 222 South Tianshui Road, Lanzhou 730000, Gansu Province, China

[b] Key Laboratory of Animal Genetics, Breeding and Reproduction of Shaanxi Province, College of Animal Science and Technology, Northwest A&F University, No. 22 Xinong Road, Yangling 712100, Shaanxi Province, China

[c] Institute of Biological and Chemical Systems, Biological Information Processing (IBCS-BIP), Karlsruhe Institute of Technology (KIT), Hermann-von-Helmholtz Platz 1, 76344 Eggenstein-Leopoldshafen, Germany

HIGHLIGHTS

- Zebrafish: a powerful model for visualizing the developmental neurotoxicity of nickel.
- Nickel exposure induces zebrafish neurodevelopmental and neurobehavioral disorders.
- Nickel exposure activates zebrafish microglia and triggers neuroimmune responses.
- Nickel exposure interferes with cerebral and somatic vasculogenesis in zebrafish.
- Ferroptosis is strongly implicated in nickel-induced neurotoxic effects.

GRAPHICAL ABSTRACT

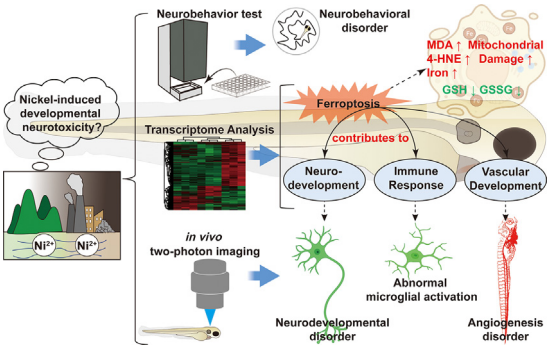

ARTICLE INFO

Editor: Henner Hollert

Keywords:
Heavy metal
Neurotoxic effects
Neurobehavioral test
In vivo two-photon imaging
RNA-sequencing
Deferoxamine

ABSTRACT

Nickel (Ni) is a widely utilized heavy metal that can cause environmental pollution and health hazards. Its safety has attracted the attention of both the environmental ecology and public health fields. While the central nervous system (CNS) is one of the main targets of Ni, its neurotoxicity and the underlying mechanisms remain unclear. Here, by taking advantage of the zebrafish model for live imaging, genetic analysis and neurobehavioral studies, we reveal that the neurotoxic effects induced by exposure to environmentally relevant levels of Ni are closely related to ferroptosis, a newly-described form of iron-mediated cell death. *In vivo* two-photon imaging, neurobehavioral analysis and transcriptome sequencing consistently demonstrate that early neurodevelopment, neuroimmune function and vasculogenesis in zebrafish larvae are significantly affected by environmental Ni exposure. Importantly, exposure to various concentrations of Ni activates the ferroptosis pathway, as demonstrated by physiological/biochemical tests, as well as the expression of ferroptosis markers. Furthermore, pharmacological intervention of ferroptosis *via* deferoxamine (DFO), a classical iron chelating agent, strongly implicates iron dyshomeostasis and ferroptosis in these Ni-induced neurotoxic effects. Thus, this study elucidates the cellular and molecular mechanisms underlying Ni neurotoxicity, with implications for our understanding of the physiologically damaging effects of other environmental heavy metal pollutants.

* Corresponding author at: School of Life Sciences, Lanzhou University, No. 222 South Tianshui Road, Lanzhou 730000, Gansu Province, China.
E-mail address: zhaohy@lzu.edu.cn (H. Zhao).

http://dx.doi.org/10.1016/j.scitotenv.2022.160078
Received 14 September 2022; Received in revised form 29 October 2022; Accepted 5 November 2022
Available online 11 November 2022

1. Introduction

The heavy metal, nickel (Ni), is abundant and widely distributed in nature. Due to its distinct physical/chemical properties, Ni has been extensively applied in the manufacturing industry including the production of stainless steel and batteries, as well as in electroplating and many other standard production processes (Beattie et al., 2017). It is an indispensable raw material for household metal products, jewelry and medical equipment, as well as the specialized material required by the aerospace and national defense industries. The exploitation and utilization of Ni has greatly promoted socio-economic development, however, a consequent progressive increase in the levels of Ni contaminating various ecosystems has inevitably led to environmental pollution and health hazards (Genchi et al., 2020). As reported in the previous studies, environmental concentrations of Ni^{2+} ranged from 0.5 to 2 mg/L (approximately 8–30 μMol/L) in polluted rivers and lakes, and the recorded highest concentration of Ni^{2+} is 183 mg/L (about 3 mMol/L) near a nickel refinery (Kienle et al., 2009).

Ni can cause atopic dermatitis by skin contact, and can be absorbed and accumulated in the kidney, lungs, liver and brain, causing multi-organ toxicity. Recently, numerous studies have reported the carcinogenicity of Ni, as well as its toxic effects on various organs (Dudek-Adamska et al., 2021; Lippmann et al., 2006; Xu et al., 2010; Yue Yang et al., 2021b). The central nervous system (CNS) is one of the main targets of Ni toxicity. Studies have shown that Ni can enter the brain *via* the blood-brain barrier or olfactory nerve pathway, accumulate in brain areas and induce cytotoxicity (He et al., 2013; Lamtai et al., 2018), causing a variety of neurological symptoms such as headache, dizziness, fatigue, memory loss, sleep disturbance and ataxia (Das et al., 2019). Animal studies have demonstrated that Ni exposure may lead to a variety of neurobehavioral abnormalities. For example, it may impair the behavior and activity of *Caenorhabditis elegans*, rodents and fish by affecting their neurotransmitter systems (He et al., 2013; Ijomone et al., 2020; Topal et al., 2015), and may significantly affect their learning/memory ability, exploration behavior and lead to anxiety or depression-like behavior patterns (He et al., 2013; Lamtai et al., 2018; Nabinger et al., 2018). Among the mechanisms implicated in Ni-induced neurotoxicity, oxidative stress, mitochondrial dysfunction and abnormal cellular energy metabolism have been proposed to play closely related and significant roles (Song et al., 2017). For instance, Ni exposure can induce the production of reactive oxygen species (ROS) in neurons, and reduce the activities of antioxidant enzymes such as superoxide dismutase (SOD) and catalase (CAT), resulting in redox imbalance and increase of toxic free radicals (Xu et al., 2010, 2011). In addition, Ni may induce mitochondrial damage and DNA (mtDNA) mutations/deletions in neurons (Xu et al., 2011, 2015). The damaged mtDNA can amplify oxidative stress by encoding defective proteins of the respiratory chain, which further produces excess ROS and converts oxidative damage into mitochondrial dysfunction (He et al., 2011; Lin and Beal, 2006). Apart from triggering an energy crisis by inducing mitochondrial damage, Ni can also reduce ATP production by affecting cellular energy metabolism in the CNS (Brant and Fabisiak, 2009; Chen and Costa, 2006; Pietruska et al., 2011). Similar to other environmental heavy metals, Ni-induced activation of apoptosis and epigenetic modifications have also been reported to play important roles in its neurotoxic effects (Adedara et al., 2020; Huang et al., 2013). Nevertheless, our understanding of Ni neurotoxicity as well as the underlying mechanisms is far from complete. The few existing studies have been mostly restricted to analyzing the effects of Ni on cultured neurons *in vitro* and have ignored the contribution of other CNS cell types as well as the interaction between different cells and structures. Therefore, there is an urgent need to explore the adverse effects of Ni on the various cellular components of the CNS *in vivo*, at an omics as well as at a more general functional level. This will contribute to a more comprehensive and systematic understanding of Ni neurotoxicity.

Zebrafish share many similarities with humans at the genomic level (Barbazuk et al., 2000; Sakai et al., 2018), as well as in terms of the development and function of the CNS (Kalueff et al., 2014). Importantly, transgenic lines exhibiting cell and tissue-specific expression of fluorescent proteins provide powerful tools for dynamically tracking various cell types, thus providing significant advantages for the study of the neurotoxicity of environmental pollutants. Ni has been reported to be close related with increased mortality, delayed hatching and altered behavioral patterns in zebrafish model. In addition, it can lead to oxidative stress, increased apoptosis and abnormal muscle development (Boran and Şaffak, 2018; Lazzari et al., 2019; Nabinger et al., 2018; Yokota et al., 2019). However, the neurotoxic effects of Ni on zebrafish model system, as well as the underlying mechanisms remain largely unknown. In this study, exploiting the advantages of the zebrafish model in genetic analysis, *in vivo* imaging and the detection of neurological function, we reveal that exposure to environmentally relevant concentrations of Ni affects early neurodevelopment, neuroimmune function and angiogenesis of zebrafish larvae. Furthermore, Ni exposure significantly activates ferroptosis, a recently described form of iron-mediated cell death which has been strongly implicated in many types of CNS injuries and diseases. In addition, based on the results of pharmacological intervention, physiological/biochemical tests and transmission electron microscope (TEM) imaging of mitochondrial morphology, we reveal a close connection between the mechanism of ferroptosis and the observed neurotoxic effects induced by Ni. We hypothesize that Ni exposure may affect the regulation of iron homeostasis and antioxidant capacity in the CNS through various pathways, and eventually lead to the activation of the ferroptosis mechanism. This study thereby contributes to further elucidating the cellular and molecular mechanisms of Ni neurotoxicity from a new perspective. It provides a theoretical basis and possible solutions for the neurodevelopmental, structural and functional impairment induced by Ni, as well as other environmental heavy metals.

2. Materials and methods

2.1. Ethics statement and zebrafish maintenance

Zebrafish husbandry and experimental procedures were reviewed and approved by the Ethics Committee of Lanzhou University (Approval No. EAF2020006) and were performed in accordance with the protocols as previously described (Westerfield, 2007; Zhao et al., 2018). All efforts were taken to minimize zebrafish suffering. Wild-type zebrafish (AB strain), transgenic *Tg* (*HuC: EGFP*) (Park et al., 2000) and *Tg* (*Flk: mCherry*) (Fouquet et al., 1997) lines were obtained from the China Zebrafish Resource Center (CZRC). The *Tg* (*ApoE: EGFP*) line (Peri and Nüsslein-Volhard, 2008) was a gift from Prof. Jiulin Du group (Institute of Neuroscience, Chinese Academy of Sciences). They were maintained in automated water circulation systems (Thmorgan) at 27.8 °C under 14 h light/10 h dark lighting conditions, and were fed twice daily with Larval AP100 (<50 μm, Zeigler Bros) from 6 to 14 dpf (days post-fertilization) and with freshly hatched brine shrimps from 15 dpf.

2.2. Zebrafish developmental toxicity assays

Zebrafish embryos were obtained from male and female adults segregated in mating tanks overnight. Mating and spawning were triggered by the light being turned on the following morning. Fertilized embryos were collected and washed with standard E3 medium within 1 h. 2 hpf (hours post-fertilization) embryos were examined under the stereomicroscope and normally developing embryos were selected for further assays. The lethal toxicity of Ni was evaluated *via* a 12-day toxicity assessment, as previously described (Kim et al., 2021). Briefly, 2 hpf zebrafish embryos were exposed to nickel chloride ($NiCl_2$, Sigma-Aldrich) at different concentrations ranging from 0 to 1 M dissolved in E3 medium, which was refreshed daily. From 6 dpf onward, zebrafish larvae were fed with Larval AP100 twice daily. The concentrations that caused 50 % mortality (LC50) of the test group on each specific day with 95 % confidence limits were calculated *via* the probit regression analysis as previously described (Gu et al., 2020).

In parallel, the developmental phenotype of zebrafish embryos exposed to $NiCl_2$ at environmentally relevant levels (0, 10, 50, 100, 500, 1000 μM) was recorded from 1 to 6 dpf using stereomicroscopy as previously described

(Ramlan et al., 2017; Wang et al., 2022; Xu et al., 2022). For example, survival and hatching were continuously monitored daily, while other developmental parameters including body length at 4 dpf, heart rate at 96 hpf, malformation rates as well as spontaneous movement of 30 hpf embryos were recorded and analyzed as previously described (Wang et al., 2022; Xu et al., 2022).

2.3. Neurobehavioral tests in zebrafish larvae

Zebrafish larvae (6 dpf, n = 12–24 in each group) without morphological abnormalities were randomly selected for neurobehavioral tests as previously described (Wang et al., 2022; Xu et al., 2022). Briefly, they were placed in 24 or 48 well-plates in the observation chamber of the DanioVision Tracking System (Noldus IT) and were allowed to adapt for 10 min. Then their locomotor activities, as well as their swimming behavior in response to alternating light-dark stimuli (5:5 min L:D) and vibration stimuli (applied every 30 s) were continuously recorded at 27.8 °C. Each test was repeated independently three times, and behavioral parameters including distance swum, velocity, cumulative duration and acceleration were analyzed by using the EthoVision XT 15.0 software (Noldus IT). The data were presented as a moving average of 12–24 fish in each group, during the whole test period, or in 1 s or 1 min time intervals.

2.4. RNA-sequencing and analyses

Zebrafish larvae (6 dpf, 50 larvae in each sample) exposed to different levels of $NiCl_2$ were collected and frozen in liquid nitrogen for 6 h. Total RNA samples were isolated by using the TRIzol Regent (Invitrogen) and were then sent to Novogene (Beijing, China) for RNA sequencing. Briefly, sequencing libraries were constructed and sequenced on an Illumina HiSeq™2500/MiSeq™ platform to generate raw reads. Raw paired-end reads were merged to remain clean reads, which were mapped to the reference zebrafish genome by using the TopHat software (Trapnell et al., 2009). FPKM (fragments per kilobase of exon per million mapped reads) of each gene was calculated by use of the HTSeq software (Putri et al., 2022). Gene expression analyses were conducted *via* edgeR (Robinson et al., 2010), filter criteria of fold-change >1.5 with p-value <0.05 were used for screening of differentially expressed genes (DEGs). GO (Gene ontology) and KEGG (Kyoto Encyclopedia of Genes and Genomes) pathway analyses were conducted by using the ClusterProfiler software, which is based on Wallenius non-central hyper-geometric distribution. GSEA (Gene set enrichment analysis) was performed based on the RNA-seq data by using the GSEA software (Subramanian et al., 2005). The RNA-seq data have been submitted to the NCBI BioSample database under accession number SAMN28205974- SAMN28205982.

2.5. Quantitative real-time PCR (qRT-PCR) analyses

Total RNA from zebrafish larvae (6 dpf, 50 larvae in each sample) was isolated by using the TRIzol Regent (Invitrogen), and cDNA was synthesized by using the cDNA Synthesis Kit (CoWin Biosciences) according to the manufacturer's instructions. qRT-PCR was performed with the SYBRGreen Master Mix (CoWin Biosciences) on the Step One Plus Real-Time PCR System (ABI), following the manufacturers' recommendations. Primer sequences of all tested genes are listed in Table S1. The relative expression levels for target genes were normalized to that of *β-actin* according to the $2^{-\Delta\Delta CT}$ method.

2.6. In vivo imaging of zebrafish central nervous and blood vascular systems

The *Tg (HuC: EGFP)*, *Tg (ApoE: EGFP)* and *Tg (Flk: mCherry)* lines were used for imaging of neurons, microglia and blood vessels, respectively in $NiCl_2$ exposed zebrafish larvae. Briefly, 6 dpf larvae without morphological abnormalities were randomly selected from each group, anesthetized with 0.01 % MS-222 (Sigma-Aldrich), and then immobilized with low melting-temperature agarose in a 27.8 °C thermal chamber. Images of the *Tg (HuC: EGFP)* larvae were taken firstly by using an epifluorescence microscope (Olympus BX51). Subsequently, a two-photon confocal laser scanning microscope (Olympus FV1000) was used to observe the morphology and cell density of neurons and microglia in the telencephalon and optic tectum region, as well as the fine vascular morphology in the cranial and truncal region of zebrafish larvae. Images were processed and analyzed by using the Image J software (NIH), and were shown in single stack or z-stacks (step size = 1.5 μm) to a depth of 75 μm. Three-dimensional (3D) reconstruction is a process of capturing the shape and appearance of cells, which is critical in the field of neuroscience. Therefore, 3D-reconstruction and further morphological analyses of neurons, microglia and blood vessels were performed by using the IMARIS V9.0.1 software (Bitplane) according to the manufacturer's instructions.

2.7. Ferroptosis related physiological/biochemical tests

2.7.1. Iron assay

The iron content was evaluated by using the Iron Assay Kit (Jiancheng). Briefly, for each sample, 50 zebrafish larvae were homogenized in PBS, and centrifuged at 3500 ×g for 10 min; the supernatant and iron chromogenic agent were transferred into a new 1.5 mL EP tube, incubated at 80 °C for 10 min; mixture was added in a 96-well plate, and the absorbance was read at 520 nm by using a microplate reader (TECAN).

2.7.2. GSH/GSSG assay

The contents of GSH and the oxidized forms of GSH (GSSG) were measured by using the GSH/GSSG Assay Kit (Beyotime). Briefly, zebrafish larvae were frozen in liquid nitrogen and ground into powder, which was deproteinized by the supplied protein removal reagent. After centrifugation at 10,000g for 10 min at 4 °C, the content of total glutathione in the supernatant was determined by ultraviolet-visible spectrophotometer analysis at 412 nm. Next, GSH in the supernatant was removed with the supplied GSH removal reagent. After reacting for 1 h at 25 °C, the content of GSSG was determined. Thus, the levels of GSH were calculated by the following formula: GSH = Total glutathione − 2 × GSSG.

2.7.3. Detection of MDA and 4-HNE

The levels of malondialdehyde (MDA) and 4-hydroxynonenal (4-HNE) were measured to evaluate ferroptosis in $NiCl_2$-exposed zebrafish larvae. Briefly, the concentrations of MDA and 4-HNE in larval lysates were measured with the MDA Assay Kit (Sigma-Aldrich), 4-HNE Assay Kit (Abcam) respectively according to the manufacturer's instructions.

2.8. Transmission electron microscope (TEM) analyses

Zebrafish larvae (6 dpf, n = 3) from each group were randomly selected and fixed by using 2.5 % glutaraldehyde. Next, the larvae were rinsed three times with 0.1 M phosphate buffer, fixed with 1 % osmic acid fixative for 2–3 h, rinsed three times with 0.1 M phosphate buffer, dehydrated through an acetone series, and embedded *via* propylene oxide in epoxy resin. Thereafter, 50 nm thick sections of the fixed brain tissue were cut and double-stained with 3 % uranyl acetate, followed by uranyl acetate and lead citrate, and then examined by using the FEI Tecnai G2 Spirit Twin TEM.

2.9. Rescue experiment by deferoxamine (DFO) co-exposure

In order to verify the involvement of ferroptosis mechanism in the Ni-induced neurodevelopmental disorders, we used the classical inhibitor of ferroptosis -deferoxamine (DFO) to validate the role of iron dyshomeostasis. Briefly, zebrafish embryos were co-exposed to $NiCl_2$ (1000 μM) and DFO (0, 1, 10, 100 μmol/L) from 1 dpf to 6 dpf, and then *in vivo* neuroimaging as well as neurobehavioral tests were performed according to the above-mentioned methods.

2.10. Statistical analyses

Statistical analyses in this study were performed by using the GraphPad Prism 8 software or RStudio (https://rstudio.com/). Data subjected to statistical tests were firstly checked for normality and homoscedasticity. If assumptions of normality and homogeneity of variance were tenable, student's *t*-test or ANOVA (analysis of variance) followed by multiple comparison post-test was used to determine significant differences. In cases where assumptions of normality and homogeneity of variance were not met, the Mann-Whitney test or the non-parametric Krustal-Wallis test followed by multiple comparison test was performed. *P* values <0.05 were considered statistically significant. Statistical differences of $p < 0.05$, $p < 0.01$ or $p < 0.001$ are represented by *, ** or ***, respectively. All detailed statistical information is summarized in Table S2.

3. Results

3.1. Nickel (Ni) exposure impairs zebrafish early development

To assess the adverse effects of Ni on zebrafish early development, newly hatched embryos were exposed to different levels of Ni^{2+}, and various physiological indexes were continuously monitored until 12 dpf (Fig. 1A). Initially, a high-throughput time-lapse imaging system was used to track the early development of zebrafish embryos. Interestingly, at different stages ranging from 30 % epiboly to the first-time tail coiling, a significant developmental retardation was recorded with increasing Ni^{2+} levels (Fig. 1B-F and Video S1). In addition, a concentration-dependent effect of Ni^{2+} on the survival rates was observed during the exposure period (Fig. S1), and the LC50 (lethal concentration 50 %) calculated at all stages were much higher than the environmentally relevant levels (0–1000 μM) selected in this study (Fig. S2). Compared with other heavy metal compounds (such as lead, cadmium, copper or mercury), Ni^{2+} is obviously less toxic to zebrafish development. Ni^{2+} induced mortality was only observed in the high-concentration groups after 7 days of continuous exposure (Fig. 1G), and no significant teratogenic effect was observed throughout the whole process. However, with a gradual increase of dosage, Ni^{2+} exerted significant concentration-dependent inhibitory effects on zebrafish hatching, heart rate and body length (Fig. 1H-K). Spontaneous tail coiling represents a crucial index to evaluate embryonic vitality during zebrafish early development. We also observed significant decrease of coiling frequency with increasing Ni^{2+} levels (Fig. 1L). Thus, our results point to a general impairment of zebrafish growth and development caused by Ni exposure at environmentally relevant levels.

3.2. Ni exposure impairs neurobehavior of zebrafish larvae

Behavioral recording which indicates the neurodevelopmental status of zebrafish larvae represents one of the most reliable types of evidence for evaluating neurotoxic effects. In this study, we performed neurobehavioral tests on 6 dpf zebrafish larvae continuously exposed to different concentrations of Ni^{2+}. During the locomotion tests, the total swimming distance, velocity and cumulative mobility of larvae treated with 1000 μM of Ni^{2+} were all significantly decreased (Fig. 2A-D). During the light-dark stimulation tests which examine the visual motor responses of zebrafish, the total swimming distance, velocity and maximum acceleration of larvae treated with 100 μM Ni^{2+} were slightly up-regulated, whereas their behavioral activities decreased significantly with the increase of Ni^{2+} level (Fig. 2E-J). During the intermittent vibration stimulation tests, the plates containing zebrafish larvae were tapped every 30 s and the larval behavior patterns were continuously monitored. As expected, the total swimming distance, velocity, cumulative mobility and maximum acceleration of Ni^{2+} exposed larvae showed very similar patterns as in the light-dark stimulation tests, which were enhanced at lower levels but were then remarkably repressed with increasing Ni^{2+} levels (Fig. 2K-P). Nevertheless, their immediate response capability to vibration stimulations was significantly inhibited upon Ni^{2+} exposure, in a concentration-dependent manner (Fig. 2Q-T). Therefore, early-life exposure to environmental levels of Ni may cause significant neurobehavioral abnormalities in zebrafish larvae.

3.3. Gene expression modulation in Ni-exposed zebrafish larvae

To further investigate the potential toxic effects of Ni on zebrafish as well as the underlying mechanisms, whole larvae (6 dpf) exposed to environmental levels of Ni^{2+} (0, 10 μM and 100 μM) during early development were analyzed by transcriptome sequencing (Fig. S3). We first determined RNA quality and quantity by the Agilent 5400 and spectrophotometer analyses, which confirmed sufficient quality to produce transcriptome sequencing libraries (Table S3). The statistics for read information from all RNA-seq libraries are presented in Tables S4,5. The error rates were lower than 0.04 %, and the GC contents ranged from 48.08 % to 49.13 % (Figs. S4,5). Besides, the total reads were 44,008,110–52,860,696 (Fig. S6), among which at least 92.86 % were mapped to the reference genome of *Danio rerio* (Fig. S7). The total reads mapped in proper pairs were over 77.39 %, and the rates of splice map ranged from 42.1 % to 44.51 %. Moreover, results of FPKM distribution were shown in Fig. S8. The results of principal component analysis (PCA) showed that the samples within the same group were highly clustered, whereas samples in different groups were significantly dispersed (Fig. 3A). In addition, Pearson correlation analysis indicated a high correlation between samples within the same group (Fig. S9A), suggesting that environmental Ni^{2+} exposure has a significant effect on the overall gene expression profiles of zebrafish larvae. Next, we performed DEG (differential expression gene) analyses, compared with the normal control group, 506 differentially expressed genes (263 up-regulated and 243 down-regulated) were detected in the low concentration group (10 μM), while 2169 differentially expressed genes (1585 up-regulated and 584 down-regulated) were detected in the high concentration group (100 μM) (Fig. 3B,C). All DEGs were selected for heatmap plotting, which have shown the significant differences between the control and Ni^{2+} exposed groups (Fig. S9B). Furthermore, 32 up-regulated and 113 down-regulated DEGs were overlapped between 10 μM and 100 μM Ni^{2+} exposed groups, respectively, as illustrated in the Venn diagrams (Fig. S9C,D).

To clarify the potential function of the identified DEGs in zebrafish upon Ni^{2+} exposure at different levels, we performed GO (Gene ontology) and KEGG (Kyoto Encyclopedia of Genes and Genomes) enrichment analyses. The DEGs of zebrafish larvae in response to 10 and 100 μM of Ni^{2+} were all assigned to GO terms closely related to neurodevelopment, neurobehavior, vascular development, immunoregulation, as well as iron ion homeostasis and iron ion binding (Fig. 3D). In addition, according to the subsequent KEGG enrichment analysis, ferroptosis and metabolism-related pathways, which includes carbon metabolism, drug and xenobiotics metabolism, fatty acid degradation, glycolysis and pyruvate metabolism *etc.*, were significantly affected in the low concentration (10 μM) group, while in the high concentration (100 μM) group, the DEGs were mainly enriched for the programmed cell death pathways including necroptosis, apoptosis and ferroptosis, lysosome and phagosome pathways, as well as the immune-related signaling pathways (Fig. 3E). Thus, both iron homeostasis regulation and ferroptosis pathways were predicated to be significantly affected in zebrafish larvae exposed to Ni at different levels, suggesting that the ferroptosis mechanism may play a crucial role in the Ni-induced toxic effects.

3.4. Ni activates microglia and impairs neuronal and vascular development of zebrafish larvae

How do these significant effects of Ni exposure on zebrafish neurobehavior and gene expression profiles reflect its influence on neuronal and vascular development, as well as immune responses? To address this question, we performed *in vivo* imaging by using the neuron, microglia and blood vessel-specific fluorescin expressing transgenic lines to test the effects of Ni^{2+} on zebrafish neurogenesis, vasculogenesis and neuroimmune responses (Fig. 4A). After continuous exposure for 5 days during early development, we observed by fluorescence microscopy that GFP expression in the brain and spinal cord region of *Tg (HuC: EGFP)* larvae was gradually

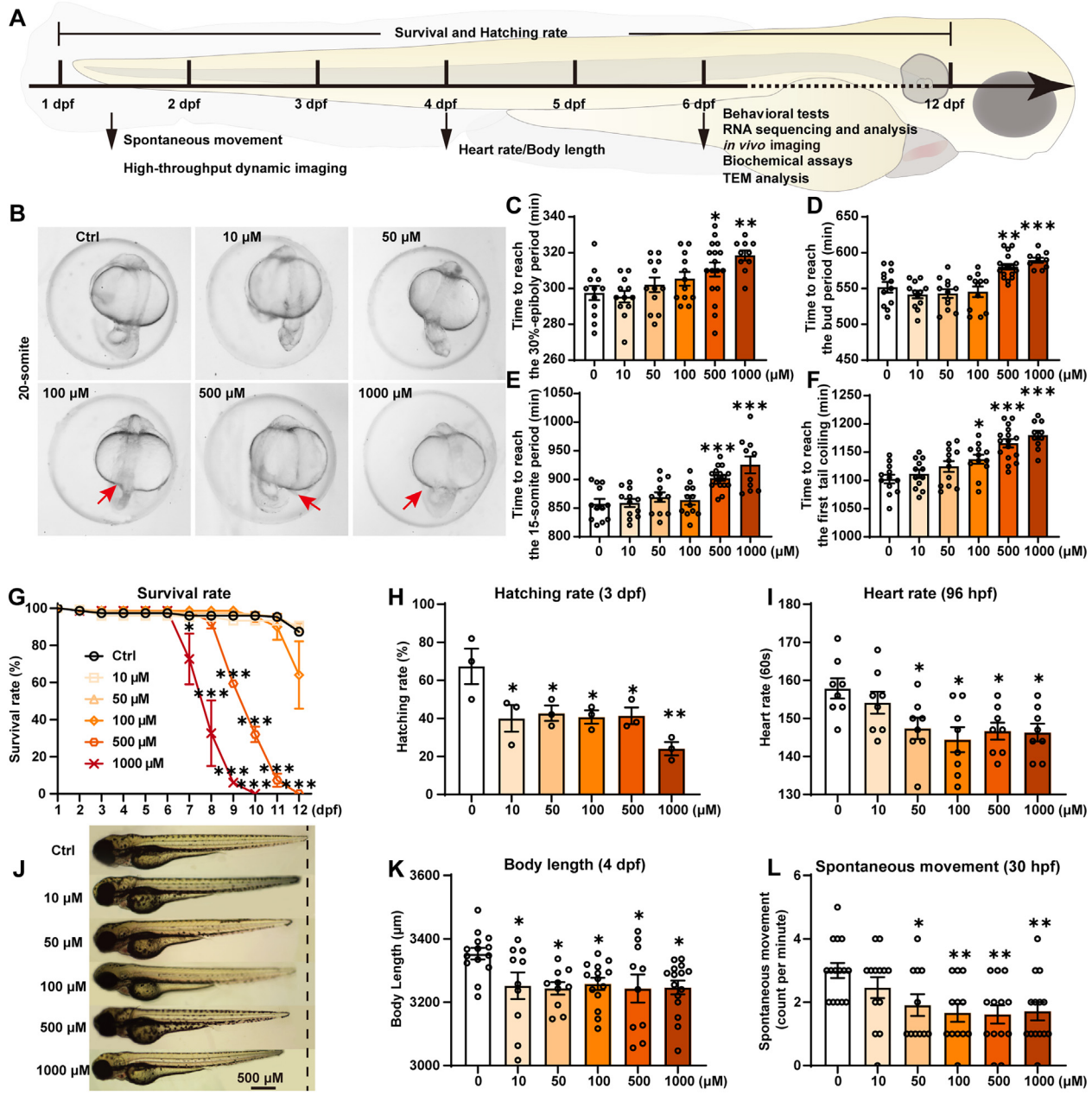

Fig. 1. Ni induces developmental toxicity in zebrafish embryos/larvae. (A) Experimental design for this study. (B—F) Representative images of high-throughput time-lapse tracking of zebrafish early development upon Ni^{2+} exposure, and the analyses of time required for embryos to reach specific developmental stages. The red arrows indicate the Ni^{2+} induced development retardation of zebrafish embryos. See also Video S1. (G) Survival rate of zebrafish embryos/larvae exposed to different levels of Ni^{2+} from 0 to 12 dpf. (H) Hatching rate of 3 dpf zebrafish larvae exposed to different concentrations of Ni^{2+}. (I) Heart rate of Ni^{2+}-exposed zebrafish larvae at 4 dpf. (J-K) Body length of Ni^{2+}-exposed zebrafish larvae at 4 dpf, and representative images indicate significant differences between Ni^{2+}-exposed and control groups. (L) Spontaneous movements of 30 hpf zebrafish larvae after Ni^{2+} exposure. Each experiment was performed independently three times. The values are presented as mean ± SEM in line chart, or as median (line), while whiskers show 90 % confidence levels in boxplots. One-way ANOVA or Kruskal-Wallis test followed by multiple comparisons test results are reported in Table S2. Significant differences are indicated by asterisks (***$p < 0.001$, **$p < 0.01$, *$p < 0.05$).

reduced with exposure to increasing Ni^{2+} levels (Fig. 4B,C). Next, we studied in detail the effects of Ni^{2+} exposure on tectal neurons by means of *in vivo* two-photon imaging. Consistent with the fluorescence imaging results, the amount and density of PVNs (periventricular neurons) in the tectal PVL (periventricular layer) region were all significantly reduced in a Ni^{2+} concentration-dependent manner (Fig. 4D,E), suggesting a distinct tendency toward a neurodevelopmental disorder, or Ni-induced neuron loss. In addition, consistent with the RNA-seq data, our qRT-PCR analyses verified that the expression profiles of neurodevelopment-related genes including *sox2*, *neurog1* and *neurog3*, were all significantly down-regulated with the increasing Ni^{2+} levels (Fig. 4F).

To investigate how exposure to Ni at environmental levels influences morphological and functional features of microglia in zebrafish, we firstly performed *in vivo* two-photon imaging of the microglia-specific *Tg (ApoE: EGFP)* line and observed that with increased Ni^{2+} levels the cerebral microglia underwent a series of transformations, changing their morphology from ramified to amoeboid (Fig. 4G). Next, 3D reconstruction of microglia and quantification of key parameters confirmed these dramatic morphological changes in response to developmental Ni^{2+} exposure, with significantly reduced surface area and volume, as well as greater sphericity, in a concentration-dependent manner (Fig. 4H-J), suggesting the notable activation of microglia and their mediated neuroimmune responses. Consistent

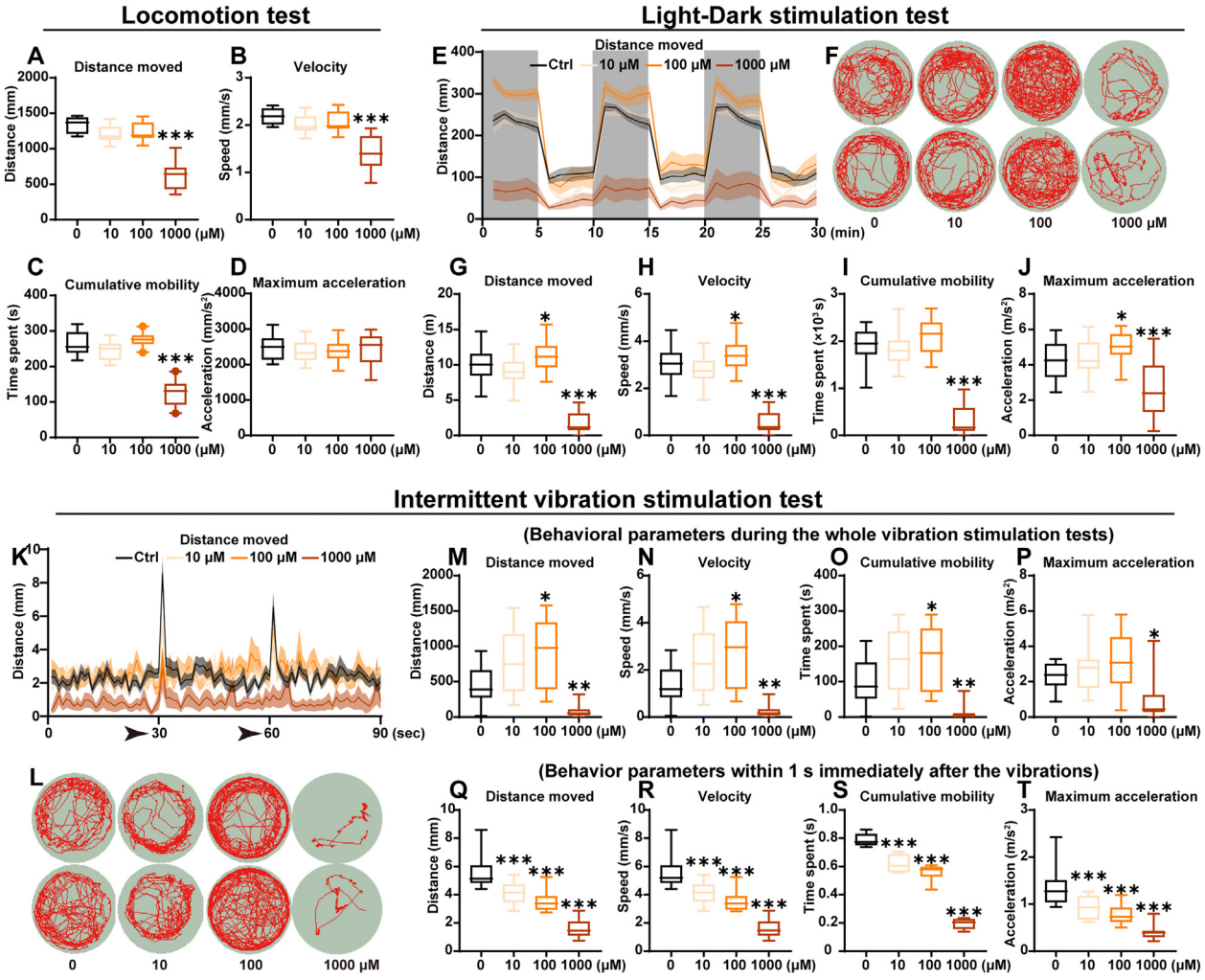

Fig. 2. Ni exposure alters neurobehavioral patterns of zebrafish larvae. (A-D) Behavior patterns of zebrafish larvae in locomotion tests. (*E*-J) Behavior patterns of zebrafish larvae in response to light-dark stimuli. (F) Representative trajectory traces of zebrafish larvae treated with Ni^{2+} during the light-dark stimulation tests. (G-J) Behavioral parameters, including swimming distance, velocity, cumulative mobility and maximum acceleration of zebrafish larvae. (K-T) Behavior patterns of zebrafish larvae in response to intermittent vibration stimuli. (L) Representative trajectory traces of zebrafish larvae treated with Ni^{2+} during the vibration stimulation tests. (M-T) Behavioral parameters, including swimming distance, velocity, cumulative mobility and maximum acceleration during the whole test (M-P) or within 1 s immediately after the vibrations as indicated by the arrows in panel K (Q-T). The values are presented as median (line), while whiskers show 90 % confidence levels in boxplots. One-way ANOVA or Kruskal-Wallis test followed by multiple comparisons test results are reported in Table S2. Significant differences are indicated by asterisks (***$p < 0.001$, **$p < 0.01$, *$p < 0.05$).

with the imaging data, both our RNA-seq and qRT-PCR analyses demonstrated that the expression of immune-related genes including *tlr1*, *il1b*, *irf3*, *nod2*, *ripk2* and *nfkb1* were all significantly up-regulated upon Ni^{2+} exposure (Fig. 4K).

Since our transcriptome data have also indicated that Ni exposure might affect angiogenesis of zebrafish larvae, we thus performed *in vivo* imaging analyses of the vascular endothelial cells (VEC) labelled transgenic *Tg (flk:mCherry)* line and observed specifically the cerebrovascular and somatic vascular networks of 6 dpf larvae. This revealed that Ni^{2+} exposure might lead to structural changes in the cerebrovascular system of zebrafish larvae, such as a significant constriction of vascular diameter of the basilar artery (BA) (Fig. 4L,M). Moreover, for the vascular networks in the body, the total number of intersegmental vessels (ISVs), the spacing between ISVs as well as the diameter of the dorsal aorta (DA) were all significantly reduced in the Ni^{2+} exposed zebrafish larvae (Fig. 4N-Q). In addition, the area of the PCV (posterior cardinal vein) region was significantly reduced to about 80 % of the normal control group in the high- concentration treatment group, and the fluorescence intensity, which can to some extent reflect the density of blood vessels, also tends to decrease in response to Ni^{2+} exposure (Fig. 4R-T). Interestingly, again the results of gene expression analyses were highly consistent with those of the *in vivo* imaging (Fig. 4U). Thus, our results point to a general depression of early angiogenesis induced by Ni exposure.

3.5. Ni exposure induces ferroptosis in zebrafish larvae

As mentioned above, our RNA-seq data showed that the ferroptosis pathway might be significantly activated in Ni-exposed zebrafish larvae. Thus, we first performed a gene set enrichment analysis (GSEA), which also demonstrated that ferroptosis-associated gene set was significantly enriched (Fig. 5A). Furthermore, the results of physiological/biochemical tests related to ferroptosis showed that the malondialdehyde (MDA), 4-Hydroxynonenal (4-HNE) and iron ion contents were increased (Fig. 5B), while the levels of total glutathione, reduced glutathione (GSH), oxidized glutathione (GSSG) and GSH/GSSG were all significantly decreased in the larvae upon Ni^{2+} exposure (Fig. 5C,D). Consistent with the RNA-seq results, the expression of genes related to ferroptosis was significantly modulated by Ni^{2+}, with the *gpx4a*, *tfr*, *ho-1* down-regulated and the *ptgs2a*, *ptgs2b*, *tf*, *fth*, *slcc7a11*, *dmt1*, *cybb* remarkably up-regulated (Fig. 5E,F). These results suggested that Ni exposure might significantly perturb iron

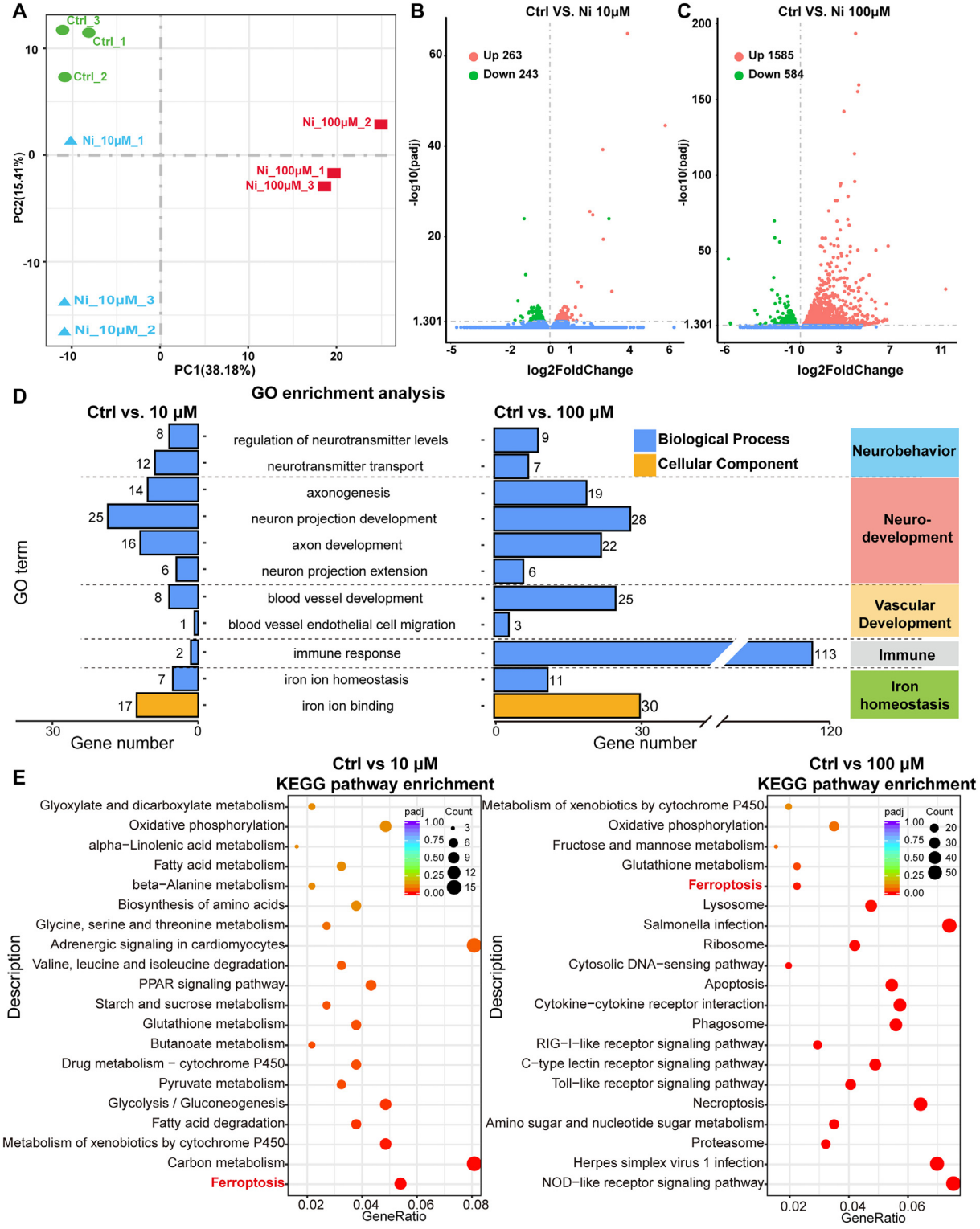

Fig. 3. Transcriptome analysis of zebrafish larvae exposed to Ni at environmentally relevant levels. (A) PCA (principal component analysis) plot. (B—C) Volcano plots illustrating the distribution of DEGs (differentially expressed genes) in zebrafish larvae treated with Ni^{2+} (0, 10, 100 μM). Each dot represents one gene. Green dots represent down-regulated DEGs; red dots represent up-regulated DEGs; blue dots represent genes that were not differentially expressed. (D-E) GO (Gene ontology) and KEGG (Kyoto Encyclopedia of Genes and Genomes) pathway enrichment analyses of Ni induced DEGs. (D) Histogram for GO enrichment analysis of DEGs in zebrafish larvae exposed to different levels of Ni^{2+}, with the numbers of DEGs indicated. (E) The top 20 significantly enriched KEGG pathways in zebrafish larvae in response to Ni^{2+} at different levels. Ferroptosis pathway is highlighted in bubble diagrams.

homeostasis and trigger ferroptosis in zebrafish larvae (Fig. 5G). Finally, to investigate whether Ni^{2+} can induce ferroptosis related morphological changes in mitochondria of brain tissues, we observed brain sections of Ni^{2+} exposed zebrafish larvae by means of the transmission electron microscopy (TEM). Interestingly, in sharp contrast to the normal control group, Ni^{2+}-exposed zebrafish larvae possessed an increased number of damaged mitochondria (with irregular matrix, disrupted membrane, or degenerated cristae) (Fig. 5H). Specifically, the subsequent quantitative

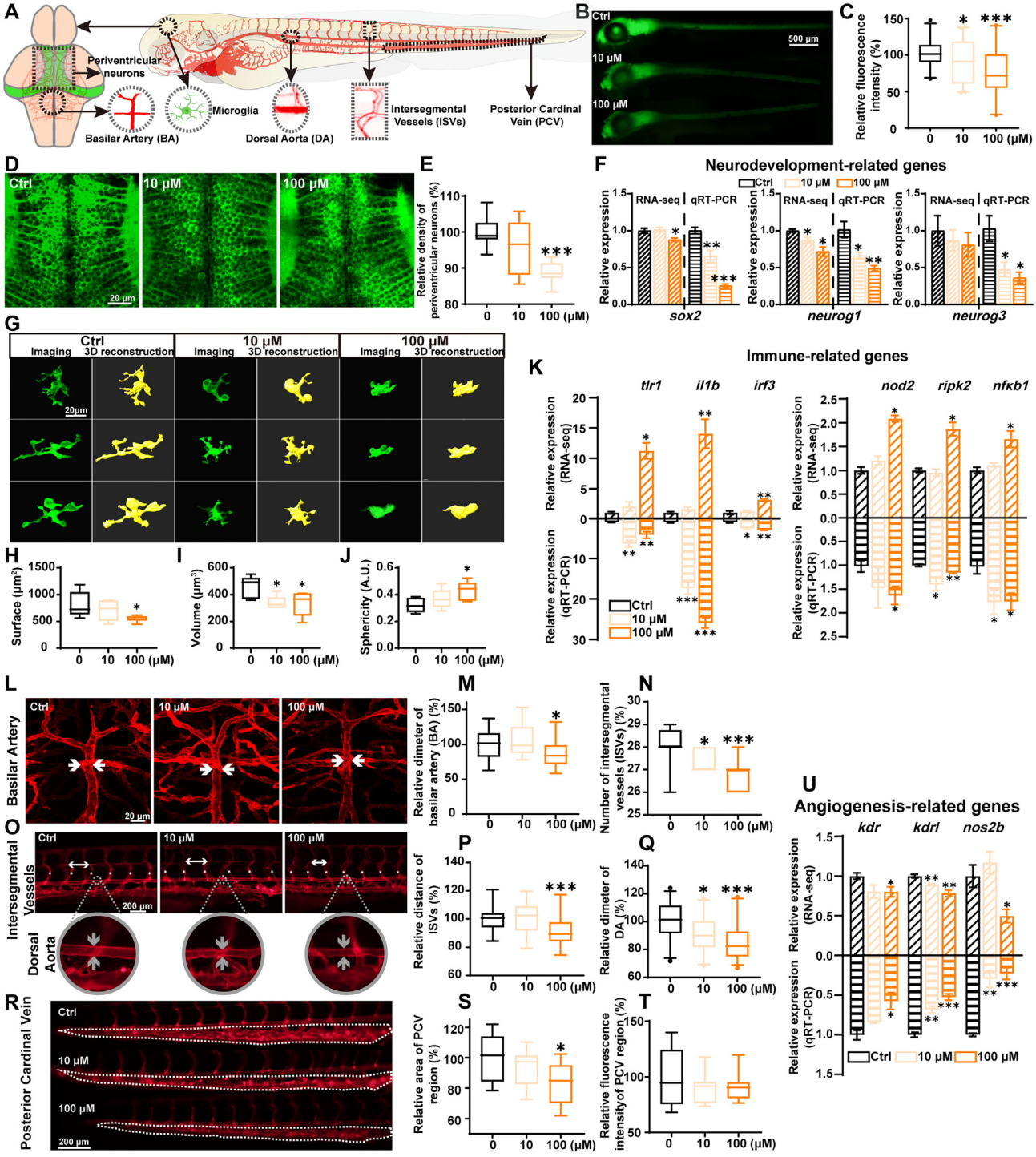

Fig. 4. Ni activates microglia and impairs neuronal and vascular development of zebrafish larvae. (A) Illustration of CNS and vascular networks of zebrafish larvae analyzed in this study. (B—C) Representative images and relative intensity of EGFP expression of 6 dpf *Tg (HuC: EGFP)* zebrafish larvae. (D-E) Representative images of the tectal periventricular layer (PVL) and neuropil region in zebrafish larvae and statistics of the relative density of periventricular neurons (PVNs). (F) RNA-seq analysis and qRT-PCR verification of gene expression related to neurodevelopment. (G-J) Morphological changes of microglia in *Tg (ApoE: EGFP)* larvae, as shown by *in vivo*-imaging, 3D reconstruction and quantification. (K) RNA-seq analysis and qRT-PCR verification of gene expression related to microglia activation and neuroinflammation. (L-M) Representative images and diameter quantifications of the basilar artery (BA) in the brain of 6 dpf *Tg (Flk: EGFP)* larvae. (N) Quantification of the number of intersegmental vessels (ISVs) in each larva. (O-Q) Representative images and quantification of the distance of ISVs and diameter of DA in zebrafish larvae. (R-T) Representative fluorescence images of the posterior cardinal vein (PCV) region and quantification of its relative area and fluorescence intensity. (U) RNA-seq analysis and qRT-PCR verification of gene expression related with angiogenesis. The values are presented as the mean ± SEM in histograms, or as median (line), while whiskers show 90 % confidence levels in boxplots. Unpaired *t*-test, One-way ANOVA or Kruskal-Wallis test followed by multiple comparisons test results are reported in Table S2. Significant differences are indicated by asterisks (***$p < 0.001$, **$p < 0.01$, *$p < 0.05$).

analyses showed that the percentage of damaged mitochondria, were all increased in the Ni^{2+} exposed groups (Fig. 5I-K). Furthermore, both the relative size and length of mitochondria tended to be decreased upon Ni^{2+} treatment (Fig. 5L-N). Collectively, all these results support our RNA-seq data that the mechanism of ferroptosis is closely involved in the Ni-induced neurotoxicity.

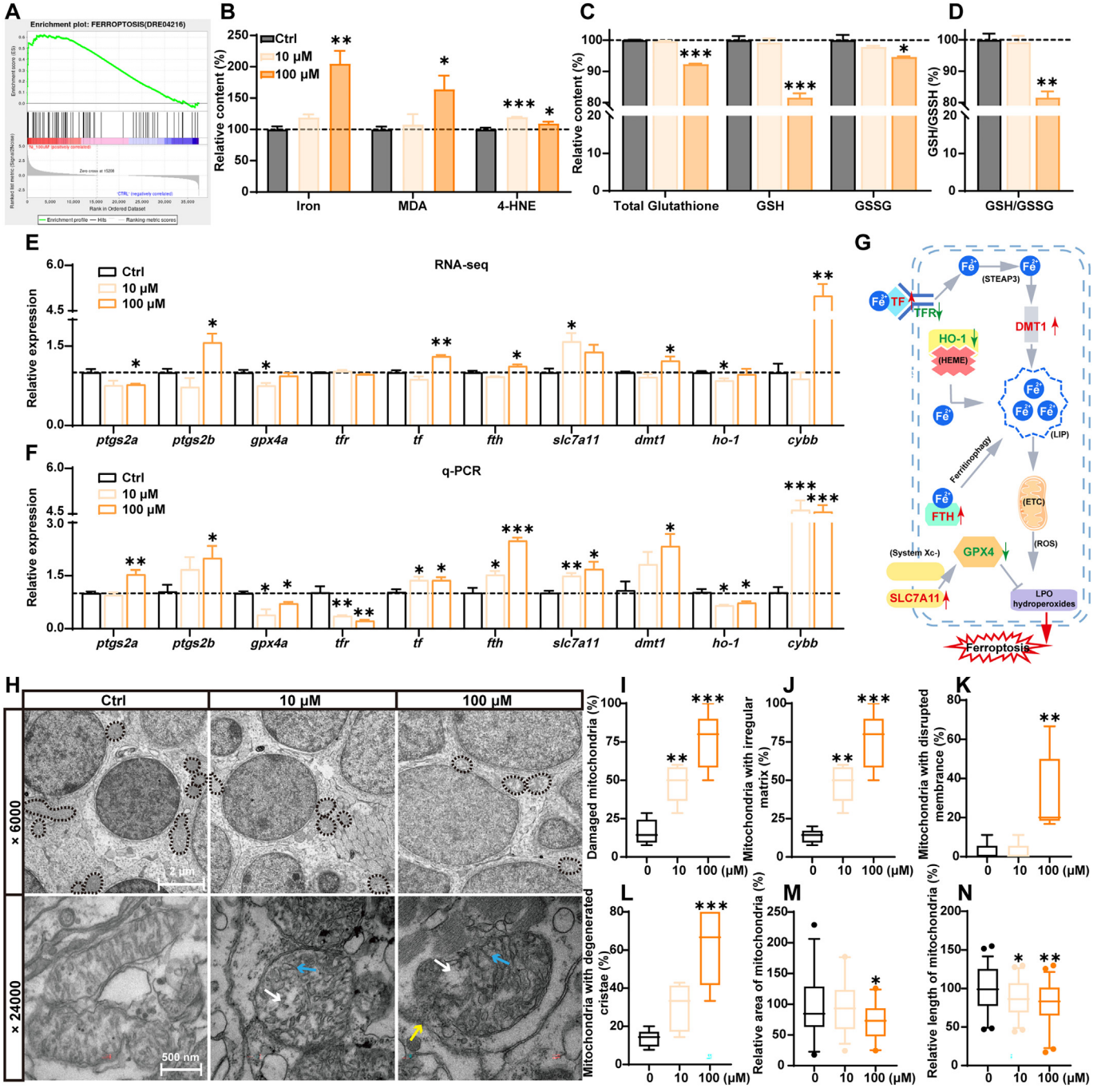

Fig. 5. Environmental Ni exposure induces ferroptosis in zebrafish larvae. (A) GSEA (Gene set enrichment analysis) of ferroptosis associated genes in 6 dpf zebrafish larvae exposed to Ni^{2+}. (B) Relative iron contents, MDA and 4HNE levels, (C) total glutathione, GSH, GSSG levels and (D) GSH/GSSG ratio in zebrafish larvae upon Ni^{2+} exposure. (*E*-F) RNA-seq analysis and qRT-PCR verification of gene expression related to iron homeostasis and ferroptosis. (G) Schematic diagram of the mechanisms underlying ferroptosis activation. (H) The mitochondrial morphology in zebrafish brain observed *via* transmission electron microscopy. The percentage of (I) damaged mitochondria and the ones with (J) irregular matrix (blue arrow indicated), (K) disrupted outer membrane (yellow arrow), and (L) degenerated cristae (white arrow), and the relative area (M) and length (N) of all mitochondria were analyzed. The values are presented as mean ± SEM in histograms, or as median (line), while whiskers show 90 % confidence levels in boxplots. Unpaired *t*-test, One-way ANOVA or Kruskal-Wallis test followed by multiple comparisons test results are reported in Table S2. Significant differences are indicated by asterisks (***$p < 0.001$, **$p < 0.01$, *$p < 0.05$).

3.6. DFO rescues the abnormal neurobehavior of Ni exposed zebrafish larvae

We next questioned whether the elevated level of ferroptosis was the cause or consequence of the Ni-induced neurotoxicity. To address this issue, we used a pharmacological approach. To specifically reduce the ferroptosis and imbalance of iron homeostasis caused by Ni exposure, zebrafish embryo/larvae were co-exposed with deferoxamine (DFO), a classical iron chelating agent together with Ni^{2+} during development. The concentrations of DFO (0, 1, 10, 100 μmol/L) used in this study were chosen according to previous studies (Chen et al., 2014; Hamilton et al., 2014). Interestingly, in the locomotion tests, DFO co-treatment significantly restored the abnormal neurobehavior (as indicated by distance moved, velocity, cumulative mobility and maximum acceleration) caused by developmental Ni^{2+} (1 mM) exposure (Fig. 6A-D). Very similar results were obtained in the light-dark stimulation tests (Fig. 6E-J). In the intermittent vibration stimulation tests, DFO co-exposure not only improved the

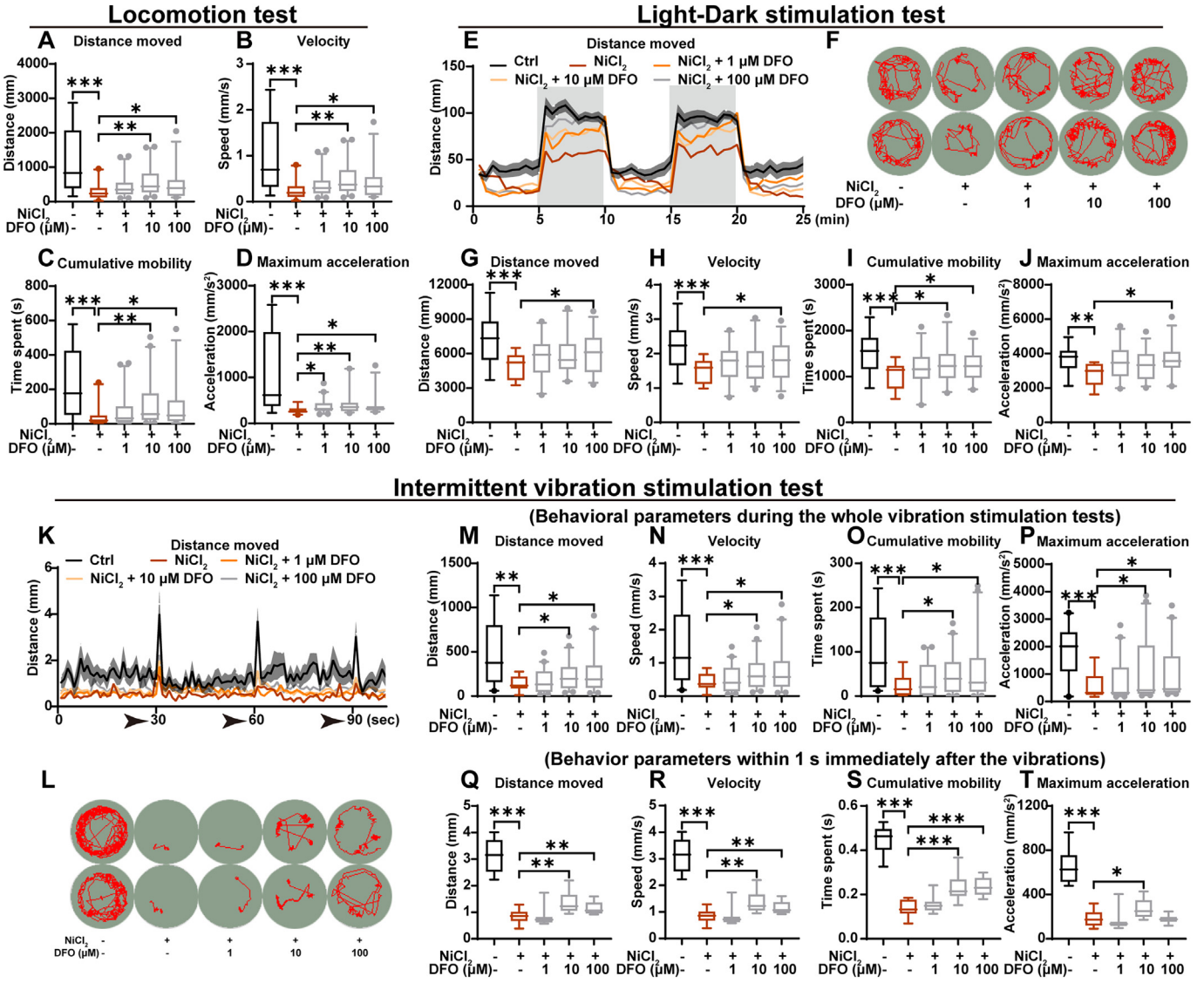

Fig. 6. DFO attenuates neurobehavioral damage induced by Ni exposure in zebrafish larvae. (A-D) Behavioral parameters of zebrafish locomotion, including swimming distance, velocity, cumulative mobility and maximum acceleration. (E-J) Behavioral patterns of zebrafish larvae in response to light-dark stimuli. (F) Representative trajectory traces of zebrafish larvae treated with Ni during the light-dark stimulation tests. (G-J) Behavioral parameters, including swimming distance, velocity, cumulative mobility and maximum acceleration of zebrafish larvae. (K-T) Behavior patterns of zebrafish larvae in response to intermittent vibration stimulus. (L) Representative trajectory traces of zebrafish larvae treated with Ni during the vibration stimulation tests. (M-T) Behavioral parameters, including swimming distance, velocity, cumulative mobility and maximum acceleration during the whole test (M-P) or within 1 s immediately after the vibrations as indicated by the arrows in panel K (Q-T). The values are presented as median (line), while whiskers show 90 % confidence levels in boxplots. One-way ANOVA or Kruskal-Wallis test followed by multiple comparisons test results are reported in Table S2. Significant differences are indicated by asterisks (***$p < 0.001$, **$p < 0.01$, *$p < 0.05$).

swimming capacity of Ni^{2+} exposed zebrafish larvae (Fig. 6K-P), but also significantly restored their immediate reaction capacity in response to vibration stimuli (Fig. 6Q-T).

3.7. DFO attenuates the impairment of neuronal and vascular development induced by Ni exposure

In order to explore the structural basis of these apparent rescue effects of DFO on Ni-induced neurobehavioral abnormalities, we performed *in vivo* two-photon imaging of the Ni^{2+} and DFO co-exposed zebrafish larvae and observed that co-treatment with DFO significantly attenuated the previously mentioned Ni^{2+}-induced toxic effects including decreased number of neurons (Fig. 7A,B), constriction of vascular diameter of the basilar artery (BA) and dorsal aorta (DA) (Fig. 7C-F), the reduced spacing between intersegmental vessels (ISVs) (Fig. 7G,H), as well as the area and density of vessels in the PCV (posterior cardinal vein) region (Fig. 7I-K). Nevertheless, surprisingly no significant difference was observed in the degree of Ni^{2+} induced activation of zebrafish microglia upon DFO treatment (Fig. S10A-C). Thus, blocking of the ferroptosis pathway appears to attenuate the impairment of neuronal and vascular development, as well as neurobehavioral disorders induced by developmental Ni exposure, pointing to ferroptosis representing a key element of the cellular mechanism underlying Ni-induced neurotoxicity.

4. Discussion

Nickel (Ni) has been established to pose a significant threat to ecosystems and human health. Recently, clinical trials and animal studies have indicated that Ni may induce a range of neurological disorders (Genchi et al., 2020; Song et al., 2017) whereas the underlying molecular and cellular mechanisms to date remain poorly understood. Zebrafish provides a powerful tool to study environmental pollutant-induced neurotoxicity,

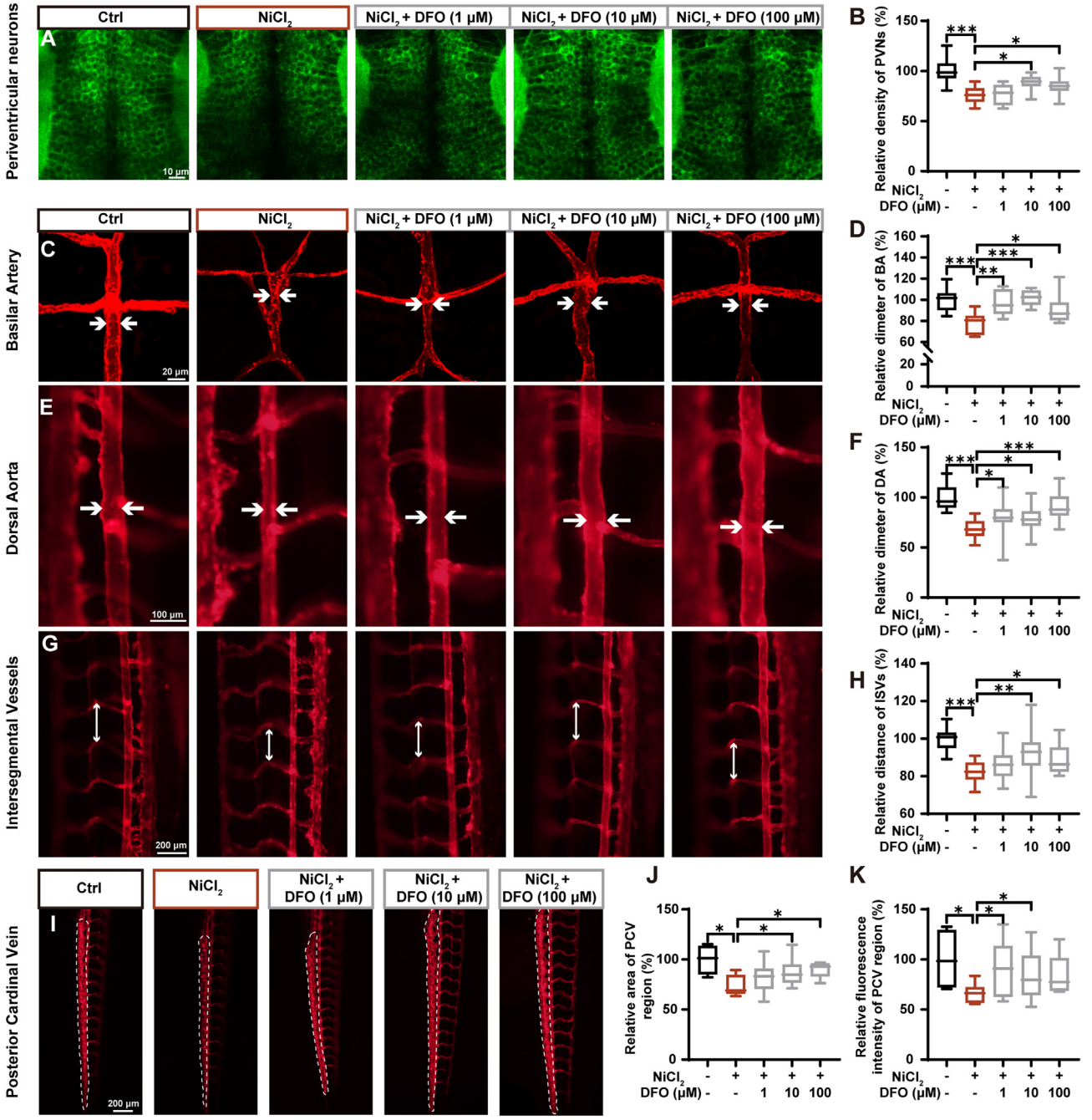

Fig. 7. DFO attenuates the impairment of neuronal and vascular development induced by Ni. (A-B) Representative images of the tectal periventricular layer (PVL) and neuropil region in zebrafish larvae and statistics of the relative density of periventricular neurons (PVNs). (C—D) Representative images and diameter quantifications of the basilar artery (BA) in the brain of 6 dpf *Tg (Flk: EGFP)* zebrafish larvae. (*E*-K) Representative images and quantifications of the distance of intersegmental vessels (ISVs), diameter of DA and the area of the posterior cardinal vein (PCV) region in zebrafish larvae. The values are presented as median (line), while whiskers show 90 % confidence levels in boxplots. One-way ANOVA or Kruskal-Wallis test followed by multiple comparisons test results are reported in Table S2.

given its similarity with humans at the genomic level as well as in terms of its general cerebral structure and function (Barbazuk et al., 2000; Sakai et al., 2018). In this study, taking advantages of this model for high-throughput neurobehavioral assays, *in vivo* imaging, as well as genetic analysis and manipulation, we have performed an in-depth functional analysis of how Ni at environmentally relevant levels influences the vertebrate CNS.

4.1. Developmental toxicity of Ni at environmentally relevant levels

Ni can enter ecosystems through precipitates from nickel-alloys and discharged industrial effluent, resulting in increased levels in the environment (Brix et al., 2017; Wang et al., 2018). A recent study has reported that environmental concentrations of Ni range from 0.5 to 2 mg/L in polluted rivers/lakes, and even with a maximum of 183 mg/L near a Ni refinery (Kienle et al., 2009). Thus, in this study, we selected the environmentally relevant levels (0–1 mM) of Ni^{2+} to evaluate its developmental toxicity on zebrafish embryos/larvae, and further selected two relatively low concentrations (10 and 100 μM, representing 0.5 and 5 mg/L, respectively) to investigate its potential neurotoxic effects and mechanisms. Consistent with previous studies (Aldavood et al., 2020; Boran and Şaffak, 2018; Kienle et al., 2008; Nabinger et al., 2018; Yongmeng Yang et al., 2021c), during zebrafish early development, Ni exposure at the selected environmental

levels slightly affected the physiological condition of larvae including a decrease in survival after 7 days of continuous exposure, a decrease in hatching rates between 2 and 3 dpf, as well as a reduction in body length and cardiac rate at 4 dpf, in a concentration-dependent fashion, while no significant teratogenic effect was identified throughout the observation phase, suggesting its relatively low developmental toxicity for zebrafish, in comparison with other toxic heavy metals (*e.g.* lead, cadmium, copper and mercury) (Jin et al., 2021; Wang et al., 2022; Xu et al., 2022; Zhang et al., 2016). In order to be more precisely testing the effects of Ni exposure on the early development of zebrafish embryos, a high-throughput dynamic imaging system was applied to test its developmental toxicity, and a significant developmental retardation was observed upon Ni exposure, in accordance with the decrease of spontaneous tail coiling, which is also closely associated with the neurodevelopmental status of zebrafish embryos.

The developing CNS is very sensitive to environmental disturbance (Grova et al., 2019). This study investigated the effects of exposure to environmental levels of Ni on zebrafish neurobehavior, and revealed that Ni significantly perturbed larval swimming patterns and reaction capacity upon exposure to increased concentrations, which is in accordance with previous studies (Kienle et al., 2008; Nabinger et al., 2018). Ni has multiple toxic effects on organisms. For example, it can affect protein function by replacing other metals in various enzymes; it can pass through calcium channels in cell membranes and competitively bind to calcium-specific receptors and furthermore, DNA damage and epigenetic modifications can be induced by the accumulation of ROS or the generation of free radicals through interfering with the antioxidant systems (Genchi et al., 2020).

4.2. Ni exposure impairs zebrafish neurodevelopment and neurovascular unit development

In this study, the detailed molecular mechanisms involved in Ni-induced toxicity were investigated *via* RNA-seq. Genes related to neurobehavior and neurodevelopment were significantly modulated in Ni-exposed larvae as indicated by the GO enrichment analysis. For example, the neurodevelopment-related genes including *sox2*, *neurog1* and *neurog3* (Flasse et al., 2013; Gong et al., 2020; Hoijman et al., 2017) all exhibited reduced expression upon Ni exposure, which may lead to abnormal development and differentiation of neurons. Further, we verified the effects of Ni on zebrafish neurodevelopment *via in vivo* imaging and observed that the number of EGFP labelled neurons, and specifically the number of periventricular neurons in the tectal region were significantly decreased, which was consistent with our behavioral and transcriptomic data.

The neurovascular unit (NVU) is a basic unit consisting of neurons as the core component together with vessels, microglia and pericytes (Willis, 2011; Zlokovic, 2011). The advantage of studying the NVU rather than neurons alone is that it encompasses the interactions between neurons and other cell types in the context of a 3D structure (Schaeffer and Iadecola, 2021; Sweeney et al., 2016). Microglia are the chief intrinsic contributors to the neuroinflammatory response among the intrinsic cellular elements in the CNS (Mallard et al., 2019; Tremblay et al., 2011), which participate in NVU dynamics to maintain CNS homeostasis (Thurgur and Pinteaux, 2019) and are considered to be one of the key factors affecting neurological function (Bachiller et al., 2018). In our RNA-seq analysis, genes related to immune responses were enriched in Ni exposed larvae, therefore we speculated that microglia and their associated neuroimmune responses might also be significantly affected. Gene expression analyses and *in vivo* imaging demonstrated that the developmental Ni exposure triggered the expression of neuroinflammation-related genes and the appearance of amoebocyte-like microglia. These observations are consistent with zebrafish microglia being vulnerable to environmental Ni exposure (Kwon and Koh, 2020; Perry et al., 2010). Blood vessels are another key component of the NVU which supplies nutrients and oxygen to other cell types in the CNS. In our transcriptomics analysis, the expression of angiogenesis-related genes was significantly modified in Ni exposed larvae, of which the repression expression of *kdr*, *kdrl* and *nos2b* expression (Gao et al., 2021; Mullapudi et al., 2019) has been verified by qRT-PCR assays. Furthermore, *in vivo* imaging of vascular morphology revealed abnormal angiogenesis of the cerebrovascular and trunk-vascular system in Ni exposed larvae, which may in turn affect early growth and development of zebrafish (Campinho et al., 2020; Paulissen et al., 2022).

4.3. Ferroptosis contributes to Ni-induced developmental neurotoxicity

According to previous studies, Ni can induce CNS injury through oxidative stress, mitochondrial dysfunction, abnormal cellular energy metabolism, apoptosis and epigenetic modifications (Genchi et al., 2020; Song et al., 2017). However, more studies are required to elucidate in detail the mechanisms which underlie this Ni-induced developmental neurotoxicity. Ferroptosis represents an important form of regulatory cell death and plays a key role in various CNS injury responses and diseases. KEGG analyses of our transcriptome data have shown that exposure to different concentrations of Ni significantly activates the ferroptosis pathway of zebrafish. The expression of genes involved in the apoptosis and necrosis pathways was significantly modulated only in the groups exposed to the highest concentrations of Ni, suggesting that ferroptosis may play a crucial role in Ni-induced toxic effects. Importantly, we identified the expression of several key factors related to ferroptosis being significantly modulated upon Ni exposure. Among these genes, *Ptgs2a/b* are a biomarkers of ferroptosis which were significantly increased in cells exposed to ferroptosis inducers (Chen et al., 2021); *tfr*, *tf*, *dmt1* and *fth* encode key factors to maintain iron homeostasis. SLC7A11, GPX4 and HO-1 are the important factors to modulate lipid-peroxidation response. Specifically, *slc7a11* is a key gene that regulate ferroptosis by enhancing GPX4 output (Xu et al., 2021), and GPX4 is a key enzyme to mitigate ferroptosis by converting lipid hydroperoxides to lipid alcohols in membranes. (Forcina and Dixon, 2019; Lei et al., 2019; Yang et al., 2014); HO-1, as another mediator of ferroptosis, can be controlled by the axis of Nrf2/SLC7A11/HO-1 to regulate cellular redox homeostasis and iron content (Chang et al., 2018; Feng et al., 2021; Z. Tang et al., 2021b); Besides, CYBB (NOX2) is the main NOX subtype that produces and accumulates ROS, ultimately leading to cellular ferroptosis (Meng et al., 2018; Ralto et al., 2020; Q. Yang et al., 2021a). In addition, our biochemical analysis showed that the content of iron, 4-HNE, MDA were all significantly increased, and the levels of GSH and GSSG were decreased in Ni exposed larvae. Mitochondrial damage is also one of the significant characteristics of ferroptosis (Li et al., 2021). TEM was used to observe the ultrastructure of mitochondria and the results demonstrated that Ni-exposed larvae possessed increased numbers of damaged mitochondria in the brain. Thus, the results obtained from examining various biomarkers are consistent with iron dyshomeostasis and ferroptosis (Liu et al., 2021; Qin et al., 2020) occurring in Ni-exposed zebrafish larvae. Interestingly, ferroptosis has also been identified in the liver of mice following exposure to Ni (Wei et al., 2022), indicating that it may play a central role in Ni-induced toxicity. Based on the above evidence, we speculate that the observed neurotoxic effects of Ni are closely related to the ferroptosis mechanism. Importantly, Ni-induced neurobehavioral disorders, as well as the observed impairments of neuronal and vascular development, could be significantly rescued by DFO treatment, a classical iron chelating agent which can inhibit the onset of ferroptosis (D. Tang et al., 2021a). However, DFO co-exposure did not exert any significant attenuating effect on Ni-induced microglia activation, suggesting that mechanisms other than ferroptosis, for example, hypoxia or redox imbalance, might also contribute to the Ni-induced microglial polarization, as well as the associated neuroinflammatory reaction.

5. Conclusions

In this zebrafish study, by using transcriptomic and neurobehavioral analysis, *in vivo* two-photon imaging as well as many physiological/biochemical assays, we reveal that exposure of developing embryos/larvaes to environmentally relevant concentrations of Ni induce significant neurobehavioral and neurodevelopmental toxicity. Briefly, Ni exposure disrupts iron homeostasis and promotes lipid peroxidation in the zebrafish CNS, activates the

ferroptosis pathway and induces various neurodevelopmental defects involving neurons, blood vessels and microglia. Thus, by documenting the involvement of a newly described form of iron-mediated cell death, this study sheds new light on the health hazards of Ni, with implications for our understanding of the neurotoxic mechanisms of Ni, as well as other environmentally relevant heavy metals.

Supplementary data to this article can be found online at https://doi.org/10.1016/j.scitotenv.2022.160078.

CRediT authorship contribution statement

Zuo Wang: Investigation, Methodology, Formal analysis, Writing – original draft. **Kemin Li:** Investigation. **Yanyi Xu:** Investigation. **Zan Song:** Investigation. **Xianyong Lan:** Resources. **Chuanying Pan:** Resources. **Shengxiang Zhang:** Resources, Supervision. **Nicholas S. Foulkes:** Resources, Supervision, Writing – review & editing. **Haiyu Zhao:** Conceptualization, Methodology, Investigation, Validation, Project administration, Resources, Funding acquisition, Supervision, Writing – review & editing.

Data availability

Data will be made available on request.

Declaration of competing interest

The authors declare no competing financial interest.

Acknowledgments

This study was supported by the National Natural Science Foundation of China (Grant No. 32100376), the Fundamental Research Funds for the Central Universities (No. lzujbky-2019-74) and the "Double First-Class" Research Start-up Funds of Lanzhou University (No. 561119203) for Dr. Haiyu Zhao, and the Helmholtz funding program Natural, Artificial and Cognitive Information Processing (NACIP) for Prof. Dr. Nicholas S. Foulkes. We thank Prof. Dr. Jiulin Du for his generous gift of transgenic zebrafish line. We also would like to thank the China Zebrafish Resource Center (CZRC) and the Research and Experiment Center of School of Life Sciences in Lanzhou University. We are grateful to the editor and reviewers for their helpful comments to greatly improve the quality of the paper.

References

Adedara, I.A., Adegbosin, A.N., Abiola, M.A., Odunewu, A.A., Owoeye, O., Owumi, S.E., Farombi, E.O., 2020. Neurobehavioural and biochemical responses associated with exposure to binary waterborne mixtures of zinc and nickel in rats. Environ. Toxicol. Pharmacol. 73, 103294. https://doi.org/10.1016/j.etap.2019.103294.

Aldavood, S.J., Abbott, L.C., Evans, Z.R., Griffin, D.J., Lee, M.D., Quintero-Arevalo, N.M., Villalobos, A.R., 2020. Effect of cadmium and nickel exposure on early development in zebrafish (Danio rerio) embryos. Water 12, 1–16. https://doi.org/10.3390/w12113005 (Switzerland).

Bachiller, S., Jiménez-Ferrer, I., Paulus, A., Yang, Y., Swanberg, M., Deierborg, T., Boza-Serrano, A., 2018. Microglia in neurological diseases: a road map to brain-disease dependent-inflammatory response. Front. Cell. Neurosci. 12, 488. https://doi.org/10.3389/fncel.2018.00488.

Barbazuk, W.B., Korf, I., Kadavi, C., Heyen, J., Tate, S., Wun, E., Bedell, J.A., McPherson, J.D., Johnson, S.L., 2000. The syntenic relationship of the zebrafish and human genomes. Genome Res. 10, 1351–1358. https://doi.org/10.1101/gr.144700.

Beattie, H., Keen, C., Coldwell, M., Tan, E., Morton, J., McAlinden, J., Smith, P., 2017. The use of bio-monitoring to assess exposure in the electroplating industry. J. Expo. Sci. Environ. Epidemiol. 27, 47–55. https://doi.org/10.1038/jes.2015.67.

Boran, H., Şaffak, S., 2018. Comparison of dissolved nickel and nickel nanoparticles toxicity in larval zebrafish in terms of gene expression and DNA damage. Arch. Environ. Contam. Toxicol. 74, 193–202. https://doi.org/10.1007/s00244-017-0468-8.

Brant, K.A., Fabisiak, J.P., 2009. Nickel and the microbial toxin, MALP-2, stimulate proangiogenic mediators from human lung fibroblasts via a HIF-1α and COX-2–mediated pathway. Toxicol. Sci. 107, 227–237. https://doi.org/10.1093/toxsci/kfn208.

Brix, K.V., Schlekat, C.E., Garman, E.R., 2017. The mechanisms of nickel toxicity in aquatic environments: an adverse outcome pathway analysis. Environ. Toxicol. Chem. https://doi.org/10.1002/etc.3706.

Campinho, P., Lamperti, P., Boselli, F., Vilfan, A., Vermot, J., 2020. Blood flow limits endothelial cell extrusion in the zebrafish dorsal aorta. Cell Rep. 31, 107505. https://doi.org/10.1016/j.celrep.2020.03.069.

Chang, L.-C., Chiang, S.-K., Chen, S.-E., Yu, Y.-L., Chou, R.-H., Chang, W.-C., 2018. Heme oxygenase-1 mediates BAY 11–7085 induced ferroptosis. Cancer Lett. 416, 124–137. https://doi.org/10.1016/j.canlet.2017.12.025.

Chen, B., Yan, Y.L., Liu, C., Bo, L., Li, G.F., Wang, H., Xu, Y.J., 2014. Therapeutic effect of deferoxamine on iron overload-induced inhibition of osteogenesis in a zebrafish model. Calcif. Tissue Int. 94, 353–360. https://doi.org/10.1007/s00223-013-9817-4.

Chen, H., Costa, M., 2006. Effect of soluble nickel on cellular energy metabolism in A549 cells. Exp. Biol. Med. 231, 1474–1480. https://doi.org/10.1177/153537020623100905.

Chen, X., Comish, P.B., Tang, D., Kang, R., 2021. Characteristics and biomarkers of ferroptosis. Front. Cell Dev. Biol. 9. https://doi.org/10.3389/FCELL.2021.637162.

Das, K.K., Reddy, R.C., Bagoji, I.B., Das, S., Bagali, S., Mullur, L., Khodnapur, J.P., Biradar, M.S., 2019. Primary concept of nickel toxicity - an overview. J. Basic Clin. Physiol. Pharmacol. 30, 141–152. https://doi.org/10.1515/jbcpp-2017-0171.

Dudek-Adamska, D., Lech, T., Konopka, T., Kościelniak, P., 2021. Nickel content in human internal organs. Biol. Trace Elem. Res. 199, 2138–2144. https://doi.org/10.1007/s12011-020-02347-w.

Feng, X., Wang, S., Sun, Z., Dong, H., Yu, H., Huang, M., Gao, X., 2021. Ferroptosis enhanced diabetic renal tubular injury via HIF-1α/HO-1 pathway in db/db mice. Front. Endocrinol. 12, 626390. https://doi.org/10.3389/fendo.2021.626390 (Lausanne).

Flasse, L.C., Pirson, J.L., Stern, D.G., Von Berg, V., Manfroid, I., Peers, B., Voz, M.L., 2013. Ascl1b and Neurod1, instead of Neurog3, control pancreatic endocrine cell fate in zebrafish. BMC Biol. 11, 78. https://doi.org/10.1186/1741-7007-11-78.

Forcina, G.C., Dixon, S.J., 2019. GPX4 at the crossroads of lipid homeostasis and ferroptosis. Proteomics 19, e1800311. https://doi.org/10.1002/pmic.201800311.

Fouquet, B., Weinstein, B.M., Serluca, F.C., Fishman, M.C., 1997. Vessel patterning in the embryo of the zebrafish: guidance by notochord. Dev. Biol. 183, 37–48. https://doi.org/10.1006/dbio.1996.8495.

Gao, L., Penglee, R., Huang, Y., Yi, X., Wang, X., Liu, L., Gong, X., Bao, B., 2021. CRISPR/Cas9-induced nos2b mutant zebrafish display behavioral abnormalities. Genes Brain Behav. 20, e12716. https://doi.org/10.1111/gbb.12716.

Genchi, G., Carocci, A., Lauria, G., Sinicropi, M.S., Catalano, A., 2020. Nickel: human health and environmental toxicology. Int. J. Environ. Res. Public Health 17. https://doi.org/10.3390/ijerph17030679.

Gong, J., Hu, S., Huang, Z., Hu, Y., Wang, X., Zhao, J., Qian, P., Wang, C., Sheng, J., Lu, X., Wei, G., Liu, D., 2020. The requirement of Sox2 for the spinal cord motor neuron development of zebrafish. Front. Mol. Neurosci. 13, 34. https://doi.org/10.3389/fnmol.2020.00034.

Grova, N., Schroeder, H., Olivier, J.-L., Turner, J.D., 2019. Epigenetic and neurological impairments associated with early life exposure to persistent organic pollutants. Int. J. Genomics 2019, 2085496. https://doi.org/10.1155/2019/2085496.

Gu, J., Wu, J., Xu, S., Zhang, L., Fan, D., Shi, L., Wang, J., Ji, G., 2020. Bisphenol F exposure impairs neurodevelopment in zebrafish larvae (Danio rerio). Ecotoxicol. Environ. Saf. 188, 109870. https://doi.org/10.1016/j.ecoenv.2019.109870.

Hamilton, J.L., Hatef, A., Imran Ul-haq, M., Nair, N., Unniappan, S., Kizhakkedathu, J.N., 2014. Clinically approved iron chelators influence zebrafish mortality, hatching morphology and cardiac function. PLoS One 9. https://doi.org/10.1371/journal.pone.0109880.

He, M.Di, Xu, S.C., Lu, Y.H., Li, L., Zhong, M., Zhang, Y.W., Wang, Y., Li, M., Yang, J., Zhang, G.Bin, Yu, Z.P., Zhou, Z., 2011. L-carnitine protects against nickel-induced neurotoxicity by maintaining mitochondrial function in neuro-2a cells. Toxicol. Appl. Pharmacol. 253, 38–44. https://doi.org/10.1016/j.taap.2011.03.008.

He, M.Di, Xu, S.C., Zhang, Xin, Wang, Y., Xiong, J.C., Zhang, Xiao, Lu, Y.H., Zhang, L., Yu, Z.P., Zhou, Z., 2013. Disturbance of aerobic metabolism accompanies neurobehavioral changes induced by nickel in mice. Neurotoxicology 38, 9–16. https://doi.org/10.1016/j.neuro.2013.05.011.

Hoijman, E., Fargas, L., Blader, P., Alsina, B., 2017. Pioneer neurog1 expressing cells ingress into the otic epithelium and instruct neuronal specification. elife 6. https://doi.org/10.7554/eLife.25543.

Huang, J., Cui, H., Peng, X., Fang, J., Zuo, Z., Deng, J., Wu, B., 2013. The association between splenocyte apoptosis and alterations of Bax, Bcl-2 and caspase-3 mRNA expression, and oxidative stress induced by dietary nickel chloride in broilers. Int. J. Environ. Res. Public Health 10, 7310–7326. https://doi.org/10.3390/ijerph10127310.

Ijomone, O.M., Miah, M.R., Akingbade, G.T., Bucinca, H., Aschner, M., 2020. Nickel-induced developmental neurotoxicity in C. elegans includes cholinergic, dopaminergic and GABAergic degeneration, altered behaviour, and increased SKN-1 activity. Neurotox. Res. 37, 1018–1028. https://doi.org/10.1007/s12640-020-00175-3.

Jin, X., Liu, W., Miao, J., Tai, Z., Li, L., Guan, P., Liu, J.-X., 2021. Copper ions impair zebrafish skeletal myofibrillogenesis via epigenetic regulation. FASEB J. 35, e21686. https://doi.org/10.1096/fj.202100183R.

Kalueff, A.V., Stewart, A.M., Gerlai, R., 2014. Zebrafish as an emerging model for studying complex brain disorders. Trends Pharmacol. Sci. 35, 63–75. https://doi.org/10.1016/j.tips.2013.12.002.

Kienle, C., Köhler, H.R., Filser, J., Gerhardt, A., 2008. Effects of nickel chloride and oxygen depletion on behaviour and vitality of zebrafish (Danio rerio, Hamilton, 1822) (Pisces, Cypriniformes) embryos and larvae. Environ. Pollut. 152, 612–620. https://doi.org/10.1016/j.envpol.2007.06.069.

Kienle, C., Köhler, H.R., Gerhardt, A., 2009. Behavioural and developmental toxicity of chlorpyrifos and nickel chloride to zebrafish (Danio rerio) embryos and larvae. Ecotoxicol. Environ. Saf. https://doi.org/10.1016/j.ecoenv.2009.04.014.

Kim, C., Choe, H., Park, J., Kim, G., Kim, K., Jeon, H.J., Moon, J.K., Kim, M.J., Lee, S.E., 2021. Molecular mechanisms of developmental toxicities of azoxystrobin and pyraclostrobin toward zebrafish (Danio rerio) embryos: visualization of abnormal development using two transgenic lines. Environ. Pollut. 270, 116087. https://doi.org/10.1016/j.envpol.2020.116087.

Kwon, H.S., Koh, S.-H., 2020. Neuroinflammation in neurodegenerative disorders: the roles of microglia and astrocytes. Transl. Neurodegener. 9, 42. https://doi.org/10.1186/s40035-020-00221-2.

Lamtai, M., Chaibat, J., Ouakki, S., Zghari, O., Mesfioui, A., El Hessni, A., Rifi, E.H., Marmouzi, I., Essamri, A., Ouichou, A., 2018. Effect of chronic administration of nickel on affective and cognitive behavior in male and female rats: possible implication of oxidative stress pathway. Brain Sci. 8. https://doi.org/10.3390/brainsci8080141.

Lazzari, M., Bettini, S., Milani, L., Maurizii, M.G., Franceschini, V., 2019. Differential nickel-induced responses of olfactory sensory neuron populations in zebrafish. Aquat. Toxicol. 206, 14–23. https://doi.org/10.1016/j.aquatox.2018.10.011.

Lei, P., Bai, T., Sun, Y., 2019. Mechanisms of ferroptosis and relations with regulated cell death: a review. Front. Physiol. 10, 1–13. https://doi.org/10.3389/fphys.2019.00139.

Li, C., Zhang, Y., Liu, J., Kang, R., Klionsky, D.J., Tang, D., 2021. Mitochondrial DNA stress triggers autophagy-dependent ferroptotic death. Autophagy 17, 948–960. https://doi.org/10.1080/15548627.2020.1739447.

Lin, M.T., Beal, M.F., 2006. Mitochondrial dysfunction and oxidative stress in neurodegenerative diseases. Nature 443, 787–795. https://doi.org/10.1038/nature05292.

Lippmann, M., Ito, K., Hwang, J.-S., Maciejczyk, P., Chen, L.-C., 2006. Cardiovascular effects of nickel in ambient air. Environ. Health Perspect. 114, 1662–1669. https://doi.org/10.1289/ehp.9150.

Liu, P., Yuan, J., Feng, Y., Chen, X., Wang, G., Zhao, L., 2021. Ferroptosis contributes to isoflurane-induced neurotoxicity and learning and memory impairment. Cell Death Discov. 7. https://doi.org/10.1038/s41420-021-00454-8.

Mallard, C., Tremblay, M.E., Vexler, Z.S., 2019. Microglia and neonatal brain injury. Neuroscience 405, 68–76. https://doi.org/10.1016/j.neuroscience.2018.01.023.

Meng, X.-M., Ren, G.-L., Gao, L., Yang, Q., Li, H.-D., Wu, W.-F., Huang, C., Zhang, L., Lv, X.-W., Li, J., 2018. NADPH oxidase 4 promotes cisplatin-induced acute kidney injury via ROS-mediated programmed cell death and inflammation. Lab. Investig. 98, 63–78. https://doi.org/10.1038/labinvest.2017.120.

Mullapudi, S.T., Boezio, G.L.M., Rossi, A., Marass, M., Matsuoka, R.L., Matsuda, H., Helker, C.S.M., Yang, Y.H.C., Stainier, D.Y.R., 2019. Disruption of the pancreatic vasculature in zebrafish affects islet architecture and function. Development 146. https://doi.org/10.1242/dev.173674.

Nabinger, D.D., Altenhofen, S., Bitencourt, P.E.R., Nery, L.R., Leite, C.E., Vianna, M.R.M.R., Bonan, C.D., 2018. Nickel exposure alters behavioral parameters in larval and adult zebrafish. Sci. Total Environ. 624, 1623–1633. https://doi.org/10.1016/j.scitotenv.2017.10.057.

Park, H.C., Kim, C.H., Bae, Y.K., Yeo, S.Y., Kim, S.H., Hong, S.K., Shin, J., Yoo, K.W., Hibi, M., Hirano, T., Miki, N., Chitnis, A.B., Huh, T.L., 2000. Analysis of upstream elements in the HuC promoter leads to the establishment of transgenic zebrafish with fluorescent neurons. Dev. Biol. 227, 279–293. https://doi.org/10.1006/dbio.2000.9898.

Paulissen, E., Palmisano, N.J., Waxman, J.S., Martin, B.L., 2022. Somite morphogenesis is required for axial blood vessel formation during zebrafish embryogenesis. eLife 11, 1–29. https://doi.org/10.7554/ELIFE.74821.

Peri, F., Nüsslein-Volhard, C., 2008. Live imaging of neuronal degradation by microglia reveals a role for v0-ATPase a1 in phagosomal fusion in vivo. Cell 133, 916–927. https://doi.org/10.1016/j.cell.2008.04.037.

Perry, V.H., Nicoll, J.A.R., Holmes, C., 2010. Microglia in neurodegenerative disease. Nat. Rev. Neurol. 6, 193–201. https://doi.org/10.1038/nrneurol.2010.17.

Pietruska, J.R., Liu, X., Smith, A., McNeil, K., Weston, P., Zhitkovich, A., Hurt, R., Kane, A.B., 2011. Bioavailability, intracellular mobilization of nickel, and HIF-1α activation in human lung epithelial cells exposed to metallic nickel and nickel oxide nanoparticles. Toxicol. Sci. 124, 138–148. https://doi.org/10.1093/toxsci/kfr206.

Putri, G.H., Anders, S., Pyl, P.T., Pimanda, J.E., Zanini, F., 2022. Analysing high-throughput sequencing data in python with HTSeq 2.0. Bioinformatics https://doi.org/10.1093/bioinformatics/btac166.

Qin, X., Tang, Q., Jiang, X., Zhang, J., Wang, B., Liu, X., Zhang, Y., Zou, Z., Chen, C., 2020. Zinc oxide nanoparticles induce ferroptotic neuronal cell death in vitro and in vivo. Int. J. Nanomedicine 15, 5299–5315. https://doi.org/10.2147/IJN.S250367.

Ralto, K.M., Rhee, E.P., Parikh, S.M., 2020. NAD(+) homeostasis in renal health and disease. Nat. Rev. Nephrol. 16, 99–111. https://doi.org/10.1038/s41581-019-0216-6.

Ramlan, N.F., Sata, N.S.A.M., Hassan, S.N., Bakar, N.A., Ahmad, S., Zulkifli, S.Z., Abdullah, C.A.C., Ibrahim, W.N.W., 2017. Time dependent effect of chronic embryonic exposure to ethanol on zebrafish: morphology, biochemical and anxiety alterations. Behav. Brain Res. 332, 40–49. https://doi.org/10.1016/j.bbr.2017.05.048.

Robinson, M.D., McCarthy, D.J., Smyth, G.K., 2010. edgeR: a bioconductor package for differential expression analysis of digital gene expression data. Bioinformatics 26, 139–140. https://doi.org/10.1093/bioinformatics/btp616.

Sakai, C., Ijaz, S., Hoffman, E.J., 2018. Zebrafish models of neurodevelopmental disorders: past, present, and future. Front. Mol. Neurosci. 11. https://doi.org/10.3389/fnmol.2018.00294.

Schaeffer, S., Iadecola, C., 2021. Revisiting the neurovascular unit. Nat. Neurosci. 24, 1198–1209. https://doi.org/10.1038/s41593-021-00904-7.

Song, X., Fiati Kenston, S.S., Kong, L., Zhao, J., 2017. Molecular mechanisms of nickel induced neurotoxicity and chemoprevention. Toxicology 392, 47–54. https://doi.org/10.1016/j.tox.2017.10.006.

Subramanian, A., Tamayo, P., Mootha, V.K., Mukherjee, S., Ebert, B.L., Gillette, M.A., Paulovich, A., Pomeroy, S.L., Golub, T.R., Lander, E.S., Mesirov, J.P., 2005. Gene set enrichment analysis: a knowledge-based approach for interpreting genome-wide expression profiles. Proc. Natl. Acad. Sci. U. S. A. 102, 15545–15550. https://doi.org/10.1073/pnas.0506580102.

Sweeney, M.D., Ayyadurai, S., Zlokovic, B.V., 2016. Pericytes of the neurovascular unit: key functions and signaling pathways. Nat. Neurosci. 19, 771–783. https://doi.org/10.1038/nn.4288.

Tang, D., Chen, X., Kang, R., Kroemer, G., 2021. Ferroptosis: molecular mechanisms and health implications. Cell Res. 31, 107–125. https://doi.org/10.1038/s41422-020-00441-1.

Tang, Z., Ju, Y., Dai, X., Ni, N., Liu, Y., Zhang, D., Gao, H., Sun, H., Zhang, J., Gu, P., 2021. HO-1-mediated ferroptosis as a target for protection against retinal pigment epithelium degeneration. Redox Biol. 43, 101971. https://doi.org/10.1016/j.redox.2021.101971.

Thurgur, H., Pinteaux, E., 2019. Microglia in the neurovascular unit: blood-brain Barrier–microglia interactions after central nervous system disorders. Neuroscience 405, 55–67. https://doi.org/10.1016/j.neuroscience.2018.06.046.

Topal, A., Atamanalp, M., Oruç, E., Halıcı, M.B., Şişecioğlu, M., Erol, H.S., Gergit, A., Yılmaz, B., 2015. Neurotoxic effects of nickel chloride in the rainbow trout brain: assessment of c-Fos activity, antioxidant responses, acetylcholinesterase activity, and histopathological changes. Fish Physiol. Biochem. 41, 625–634. https://doi.org/10.1007/s10695-015-0033-1.

Trapnell, C., Pachter, L., Salzberg, S.L., 2009. TopHat: discovering splice junctions with RNA-Seq. Bioinformatics 25, 1105–1111. https://doi.org/10.1093/bioinformatics/btp120.

Tremblay, M.È., Stevens, B., Sierra, A., Wake, H., Bessis, A., Nimmerjahn, A., 2011. The role of microglia in the healthy brain. J. Neurosci. 31, 16064–16069. https://doi.org/10.1523/JNEUROSCI.4158-11.2011.

Wang, X.Q., Wei, D.P., Ma, Y.B., McLaughlin, M.J., 2018. Soil ecological criteria for nickel as a function of soil properties. Environ. Sci. Pollut. Res. 25, 2137–2146. https://doi.org/10.1007/s11356-017-0456-6.

Wang, Z., Zhao, H., Xu, Y., Zhao, J., Song, Z., Bi, Y., Li, Y., Lan, X., Pan, C., Foulkes, N.S., Zhang, S., 2022. Early-life lead exposure induces long-term toxicity in the central nervous system: from zebrafish larvae to juveniles and adults. Sci. Total Environ. 804. https://doi.org/10.1016/j.scitotenv.2021.150185.

Wei, L., Zuo, Z., Yang, Z., Yin, H., Yang, Y., Fang, J., Cui, H., Du, Z., Ouyang, P., Chen, X., Chen, J., Geng, Y., Zhu, Y., Chen, Z., Huang, C., Wang, F., Guo, H., 2022. Mitochondria damage and ferroptosis involved in Ni-induced hepatotoxicity in mice. Toxicology 466, 153068. https://doi.org/10.1016/j.tox.2021.153068.

Westerfield, M., 2007. The Zebrafish Book. A Guide for the Laboratory Use of Zebrafish (Danio rerio). 5th edition. University of Oregon Press, Eugene (Book).

Willis, C.L., 2011. Glia-induced reversible disruption of blood-brain barrier integrity and neuropathological response of the neurovascular unit. Toxicol. Pathol. 39, 172–185. https://doi.org/10.1177/0192623310385830.

Xu, F., Guan, Y., Xue, L., Zhang, P., Li, M., Gao, M., Chong, T., 2021. The roles of ferroptosis regulatory gene SLC7A11 in renal cell carcinoma: a multi-omics study. Cancer Med. 10, 9078–9096. https://doi.org/10.1002/cam4.4395.

Xu, S., He, M., Lu, Y., Li, L., Zhong, M., Zhang, Y., Wang, Y., Yu, Z., Zhou, Z., 2011. Nickel exposure induces oxidative damage to mitochondrial DNA in Neuro2a cells: the neuroprotective roles of melatonin. J. Pineal Res. 51, 426–433. https://doi.org/10.1111/j.1600-079X.2011.00906.x.

Xu, S., He, M., Zhong, M., Li, L., Lu, Y., Zhang, Y., Zhang, L., Yu, Z., Zhou, Z., 2015. The neuroprotective effects of taurine against nickel by reducing oxidative stress and maintaining mitochondrial function in cortical neurons. Neurosci. Lett. 590, 52–57. https://doi.org/10.1016/j.neulet.2015.01.065.

Xu, S.-C., He, M.-D., Zhong, M., Zhang, Y.-W., Wang, Y., Yang, L., Yang, J., Yu, Z.-P., Zhou, Z., 2010. Melatonin protects against nickel-induced neurotoxicity in vitro by reducing oxidative stress and maintaining mitochondrial function. J. Pineal Res. 49, 86–94. https://doi.org/10.1111/j.1600-079X.2010.00770.x.

Xu, Y., Zhao, H., Wang, Z., Gao, H., Liu, J., Li, K., Song, Z., Yuan, C., Lan, X., Pan, C., Zhang, S., 2022. Developmental exposure to environmental levels of cadmium induces neurotoxicity and activates microglia in zebrafish larvae: from the perspectives of neurobehavior and neuroimaging. Chemosphere 291, 132802. https://doi.org/10.1016/j.chemosphere.2021.132802.

Yang, Q., Gao, L., Hu, X.-W., Wang, J.-N., Zhang, Y., Dong, Y.-H., Lan, H.Y., Meng, X.-M., 2021. Smad3-targeted therapy protects against cisplatin-induced AKI by attenuating programmed cell death and inflammation via a NOX4-dependent mechanism. Kidney Dis. 7, 372–390. https://doi.org/10.1159/000512986 (Basel, Switzerland).

Yang, W.S., Sriramaratnam, R., Welsch, M.E., Shimada, K., Skouta, R., Viswanathan, V.S., Cheah, J.H., Clemons, P.A., Shamji, A.F., Clish, C.B., Brown, L.M., Girotti, A.W., Cornish, V.W., Schreiber, S.L., Stockwell, B.R., 2014. Regulation of ferroptotic cancer cell death by GPX4. Cell 156, 317–331. https://doi.org/10.1016/j.cell.2013.12.010.

Yang, Yongmeng, Yu, Y., Zhou, R., Yang, Yan, Bu, Y., 2021. The effect of combined exposure of zinc and nickel on the development of zebrafish. J. Appl. Toxicol. 41, 1765–1778. https://doi.org/10.1002/jat.4159.

Yang, Yue, Zuo, Z., Yang, Z., Yin, H., Wei, L., Fang, J., Guo, H., Cui, H., Ouyang, P., Chen, X., Chen, J., Geng, Y., Chen, Z., Huang, C., Zhu, Y., Liu, W., 2021. Nickel chloride induces spermatogenesis disorder by testicular damage and hypothalamic-pituitary-testis axis disruption in mice. Ecotoxicol. Environ. Saf. 225, 112718. https://doi.org/10.1016/j.ecoenv.2021.112718.

Yokota, S., Nakamura, K., Kamata, R., 2019. A comparative study of nickel nanoparticle and ionic nickel toxicities in zebrafish: histopathological changes and oxidative stress. J. Toxicol. Sci. 44, 737–751. https://doi.org/10.2131/jts.44.737.

Zhang, Q.-F., Li, Y.-W., Liu, Z.-H., Chen, Q.-L., 2016. Exposure to mercuric chloride induces developmental damage, oxidative stress and immunotoxicity in zebrafish embryos-larvae. Aquat. Toxicol. 181, 76–85. https://doi.org/10.1016/j.aquatox.2016.10.029.

Zhao, H., Di Mauro, G., Lungu-Mitea, S., Negrini, P., Guarino, A.M., Frigato, E., Braunbeck, T., Ma, H., Lamparter, T., Vallone, D., Bertolucci, C., Foulkes, N.S., 2018. Modulation of DNA repair systems in blind cavefish during evolution in constant darkness. Curr. Biol. 28, 3229–3243.e4. https://doi.org/10.1016/j.cub.2018.08.039.

Zlokovic, B.V., 2011. Neurovascular pathways to neurodegeneration in Alzheimer's disease and other disorders. Nat. Rev. Neurosci. 12, 723–738. https://doi.org/10.1038/nrn3114.